

1
2
3
4 **Assessing origins of end-Triassic tholeiites from Eastern North America using hafnium**
5 **isotopes**
6
7

8 Lynne J. Elkins^{1, *}, Christine M. Meyzen², Sara Callegaro³, Andrea Marzoli², Michael Bizimis⁴
9

10
11
12 ¹ University of Nebraska-Lincoln, Lincoln, NE 68510; lelkins@unl.edu
13

14 ² Dipartimento di Geoscienze, Università degli Studi di Padova, Via G. Gradenigo, 6, 35131
15 Padova, Italy; andrea.marzoli@unipd.it, christine.meyzen@unipd.it
16

17 ³ Centre for Earth Evolution and Dynamics, University of Oslo, Oslo, Norway;
18 sara.callegaro@geo.uio.no
19

20 ⁴ University of South Carolina; mbizimis@geol.sc.edu
21

22 * Corresponding author: Lynne Elkins (lelkins@unl.edu)
23
24
25

26 **Key Points:**

- 27
- End-Triassic tholeiites from Eastern North America were likely products of melting
28 Paleozoic age, subduction-metasomatized mantle
 - Direct melting of recycled crustal rocks may also have occurred, but cannot fully explain
29 the tholeiite isotopic compositions observed
30
 - Southern Eastern North American tholeiites likely also experienced assimilation of lower
31 continental crust, possibly intermediate granulite
32

33 **Abstract**

34 The driving processes responsible for producing the Central Atlantic Magmatic Province, the
35 Large Igneous Province associated with end-Triassic rifting of Pangea, remain largely debated.
36 Because their compositions encompass most of the Central Atlantic basalt spectrum, tholeiites
37 from southern Eastern North America are considered pivotal for identifying magma origins. New
38 $^{176}\text{Hf}/^{177}\text{Hf}$ measurements for 201 Ma Eastern North American tholeiites dominantly record a
39 local petrogenetic history. Their ϵ_{Hf} ratios, corrected to an emplacement age of 201 Ma (-7.85 to
40 +5.86), form a positive but shallowly sloped array slightly deviating from the terrestrial array on
41 a ϵ_{Hf} vs. ϵ_{Nd} diagram. Comparison of $^{176}\text{Hf}/^{177}\text{Hf}$ to other isotope ratios and trace elements helps
42 to rule out several petrogenetic scenarios, particularly mixing of melts from global depleted or
43 enriched mantle components. In contrast, partial melting of subduction-metasomatized mantle
44 can explain the parental magma composition for southern Eastern North America. Such
45 metasomatism likely occurred during Paleozoic subduction around Pangea and may have been
46 dominated by sediment-derived fluid reactions. The observed $^{176}\text{Hf}/^{177}\text{Hf}$ vs. $^{143}\text{Nd}/^{144}\text{Nd}$ array
47 may reflect subsequent assimilation of lower continental crust, perhaps together with limited
48 direct melting of recycled continental crust in the asthenosphere. The proposed recycling
49 scenario does not specifically support or preclude a mantle plume origin for the Central Atlantic
50 Magmatic Province, but instead points toward the presence of a distinct local mantle source and
51 crustal assimilation processes during magma transport. Detailed understanding of these local
52 effects is needed in order to more accurately understand the origins of Large Igneous Provinces.

53

54 **Key words:** 8410 Geochemical modeling; 8137 Hotspots, large igneous provinces, and flood
55 basalt volcanism; 1040 Radiogenic isotope geochemistry; 1037 Magma genesis and partial

57 **1. INTRODUCTION**

58 The Triassic-Jurassic rifting of Pangea and subsequent opening of the central Atlantic Ocean
59 represent a major stage of a Wilson cycle, describing the formation and destruction of oceanic
60 basins and supercontinents (Wilson, 1966). Wilson's classic model drew directly on the central
61 Atlantic basin and its history of repeated closures and reopenings as a primary example of global
62 tectonic processes. End-Triassic rifting was associated with the emplacement of one of the most
63 voluminous continental flood basalt provinces in Earth history (Figure 1), the Central Atlantic
64 Magmatic Province (CAMP; Marzoli et al., 1999), an event significant enough to have likely
65 triggered the end-Triassic mass extinction (Cirilli et al., 2009; Davies et al., 2017; Heimdal et al.,
66 2018; Hesselbo et al., 2002; Marzoli et al., 2004). Major continental rifting events in geologic
67 history are commonly associated with the eruption of a large igneous province (LIP), but the
68 causal relationships linking rifts with LIPs remain unclear. The distinction and the transition
69 between passive and active rifting models has been the object of several studies (Burov & Gerya,
70 2014; Courtillot et al., 1999; Koptev et al., 2015; Sengör & Burke, 1978), all seeking to better
71 understand what processes initiate rifting and what factors cause rifted margins to be magma-rich
72 or magma-poor (Gillard et al., 2017). Large igneous provinces may also record the arrival of
73 deep-seated mantle plumes at the base of the lithosphere, which could in turn act to initiate
74 rifting, but it has been difficult to fully reconcile plume head arrival with continental rifting
75 models in all settings (e.g., Carlson, 1991; Courtillot et al., 1999; Morgan, 1983; Saunders et al.,
76 2007).

77 One peculiarity of CAMP magmas is that they display an overall high degree of geochemical
78 heterogeneity, which has led researchers to propose diverse magma origins such as an upwelling
79 mantle plume (e.g., Cebriá et al., 2003; De Boer, 1992; Oyarzun et al., 1997; Wilson, 1997);

80 metasomatized subcontinental lithospheric mantle (SCLM) (e.g., Deckart et al., 2005; Merle et
81 al., 2011; Verati et al., 2005); and asthenosphere and/or SCLM modified by subduction-derived
82 materials (e.g., Alibert, 1985; Callegaro et al., 2013, 2017; Dorais et al., 2005; Dupuy et al.,
83 1988; Heatherington & Mueller, 1999; Marzoli et al., 2019; Merle et al., 2014; Pegram, 1990;
84 Whalen et al., 2015). This range of proposed origins was interpreted to indicate various
85 geodynamic scenarios (e.g., Marzoli et al., 2018, and references therein). As an additional source
86 of complexity, while some of the diverse magma types have been identified across the province,
87 other CAMP magma compositions vary from region to region (Marzoli et al., 2018). It remains
88 unclear whether these regional heterogeneities are derived from locally diverse asthenospheric or
89 continental lithospheric mantle sources, or inherited by assimilation of local continental
90 lithosphere by deeper, perhaps plume-derived primary magmas. Each scenario has distinct
91 implications for how end-Triassic rifting and associated LIP emplacement occurred. The
92 diversity of models further demonstrates the uncertainty about the origins of LIPs and their links
93 to continental rifts.

94 As an important component of this ongoing effort to understand the origins of CAMP, much
95 prior literature has been dedicated to the petrogenesis of CAMP basalts from Eastern North
96 America (ENA), but questions persist about the characteristics and origins of their primary melt
97 sources, and the role and importance of assimilation and crustal contamination in modifying
98 primitive melt compositions (e.g., Callegaro et al., 2013; Dorais & Tubrett, 2008; Dostal and
99 Dupuy, 1984; Dostal & Durning, 1998; Heatherington & Mueller, 1999; McHone, 2000; Merle
100 et al., 2014; Pegram, 1990; Puffer, 1992, 2001, 2003; Shellnutt et al., 2018; Tollo & Gottfried,
101 1992; Whalen et al., 2015). Because of the geochemical heterogeneity recorded by the tholeiites
102 from Georgia to Virginia in the southern part of ENA, which encompass most of the CAMP

103 geochemical spectrum, and taking advantage of the mineralogical sensitivity of the ^{176}Lu - ^{176}Hf
104 isotopic system with respect to clinopyroxene-garnet ratios, this study aims to place new
105 constraints on the formation of CAMP and of LIPs more generally.

106 **2. GEOLOGIC SETTING**

107 **2.1. Tectonic setting of CAMP**

108 The opening of the Central Atlantic oceanic basin started with end-Triassic rifting of the
109 supercontinent Pangea, an event associated with the regional emplacement of tholeiitic magmas
110 over an estimated total surface of 10^7 km² spanning present-day eastern North America, northern
111 South America, northwest Africa, and southwestern Europe (Figure 1) (Marzoli et al., 1999,
112 2018). Central Atlantic Magmatic Province emplacement occurred at ~201 Ma with a duration of
113 peak magmatic activity constrained to less than 0.6 Ma (e.g., Blackburn et al., 2013; Davies et
114 al., 2017; Deckart et al., 1997; Dunning & Hodych, 1990; Hames et al., 2000; Hodych &
115 Dunning, 1992; Jourdan et al., 2009; Knight et al., 2004; Marzoli et al., 2004, 2011, 2019;
116 Nomade et al., 2007; Sebai et al., 1991; Verati et al., 2005, 2007). At ca. 201.6 to 200.9 Ma,
117 several short-lived magmatic pulses occurred all over the CAMP and preceded continental break-
118 up by several million years (Blackburn et al., 2013; Davies et al., 2017; Knight et al., 2004).

119 **2.2. Models for CAMP formation**

120 The origins of LIPs and their relationship with continental rifting has remained a subject of long
121 standing debate (e.g., Bryan & Ernst, 2008; Carlson, 1991; Coffin & Eldholm, 1992; Kent, 1991;
122 Morgan, 1983; Saunders et al., 2007). Many studies have invoked one or more mantle plumes as
123 triggering mechanisms for CAMP rifting and magmatism, invoking heat-driven lithospheric

124 erosion and thinning, wide-scale asthenospheric upwelling and melting in a plume head, broad
125 crustal magmatic emplacement, and possible localized focusing of regional extension in response
126 to plume impingement on the overlying plate (e.g., Cebriá et al., 2003; Hill, 1991; Lizarralde &
127 Holbrook, 1997; McHone, 1978; Morgan, 1983; Oyarzun et al., 1997; Ruiz-Martínez et al.,
128 2012; White & McKenzie, 1989; Wilson, 1997).

129 However, plume evidence related to the CAMP episode is ambiguous: the central Atlantic basin
130 does not include any hotspot tracks of early Jurassic age, and dike orientations and the near-
131 synchronous onset of magmatism from Bolivia to Spain are inconsistent with a centralized,
132 radiating plume impact (e.g., Davies et al., 2017; May, 1971; McHone, 2000; Verati et al., 2005).
133 Therefore, many studies have advocated for non-plume dynamical mechanisms for triggering
134 rifting and melting (e.g., Bédard, 1992; De Min et al., 2003; Holbrook & Kelemen, 1993;
135 Holbrook et al., 1994; Kontak, 2008; McHone, 2000). These alternative models for CAMP
136 invoke other melt generation mechanisms, such as subcontinental insulation heating and edge-
137 driven convection (e.g., Anderson, 1994; Coltice et al., 2007).

138 Geochemically, most CAMP magmas exhibit signatures enriched in incompatible trace elements,
139 with combined Pb-Sr-Nd-Os radiogenic isotopes indicating the involvement of one or more long-
140 lived source reservoirs with time-integrated incompatible trace element enrichment (e.g.,
141 Callegaro et al., 2013, 2014, 2017; Marzoli et al., 2019; Merle et al., 2011, 2014; Whalen et al.,
142 2015). While these geochemical patterns could indicate melt contributions from recycled
143 material entrained in a deep mantle plume, geochemical signatures such as LILE enrichments
144 and Nb depletions in CAMP are notably arc-like (e.g., De Min et al., 2003; Deckart et al., 2005;
145 Jourdan et al., 2003; Puffer, 2001).

146 The arc-like trace element signatures observed in CAMP magmas could indicate a unique local
147 mantle source composition, or may be derived from assimilation of continental lithosphere
148 during magma transport (Alibert, 1985; Bertrand, 1991; Bertrand et al., 1982; Cebriá et al., 2003;
149 Chabou et al., 2010; De Min et al., 2003; Deckart et al., 2005; Dupuy et al., 1988; Heatherington
150 & Mueller, 1999; Iacumin et al., 2003; Jourdan et al., 2003; Papezik et al., 1988; Pegram, 1990;
151 Puffer, 1992; Ragland et al., 1992; Tollo & Gottfried, 1992; Verati et al., 2005). A plume origin
152 for the Sr-Nd-Pb isotope systematics of CAMP is likewise problematic given the lack of Atlantic
153 OIBs with comparable signatures (e.g., Janney & Castillo, 2001; Pegram, 1990). A lack of
154 primitive (picritic) magmas in CAMP is a hindrance when defining the mantle source origins for
155 the LIP, but recent isotope analyses of ENA tholeiites suggest that for the least evolved magmas,
156 a SCLM or shallow asthenospheric mantle source modified by either subduction-derived fluids
157 or direct addition of subducted and/or delaminated continental crustal material is a viable
158 scenario (Callegaro et al., 2013, 2014; Merle et al., 2014; Shelnutt et al., 2018; Whalen et al.,
159 2015).

160 **2.3. The Eastern North America study area**

161 Eastern North American CAMP (Figure 1) hosts a particularly well-documented volcanic and
162 intrusive tholeiite series, including dike swarms, sills, and basaltic flows exposed from Georgia
163 (USA) to Newfoundland (Canada). The ENA series incorporate much of the observed
164 geochemical diversity of the overall province. The major CAMP lava piles are locally associated
165 with extensional grabens and half-grabens along what is now eastern North America. The
166 Hartford-Newark-Gettysburg-Culpeper basins of Massachusetts, Connecticut, New Jersey,
167 Pennsylvania, and Virginia host a series of three major volcanic episodes, including the oldest
168 Orange Mountain series, the intermediate-age Preakness series, and the youngest Hook Mountain

169 series (e.g., Puffer, 1992; Tollo & Gottfried, 1992). These units are matched by similarly dated
170 and geochemically identified basalts and feeder dikes in Canada (e.g., Kontak, 2008; Jourdan et
171 al., 2009; Pe-Piper & Piper, 1999) and Morocco (e.g., Bertrand et al., 1982; Marzoli et al., 2019).
172 Contrary to observations in Morocco and northern ENA, rift basins in southern Virginia, the
173 Carolinas, and Georgia do not preserve lava flows and are dominated instead by diabase dikes
174 and a few sills (e.g., Ragland et al., 1992; Weigand & Ragland, 1970).

175 Diabases and basalt flows from ENA are geochemically diverse, and detailed analysis has
176 indicated that multiple parental magmas with distinct differentiation, fractionation, and/or
177 assimilation paths are likely necessary to generate the geochemical variations observed (e.g.,
178 Tollo & Gottfried, 1992). Mantle potential temperatures extrapolated from high-Fo ($> Fo_{87}$)
179 olivine cores from these rocks have a maximum calculated value of 1480°C (Callegaro et al.,
180 2013; Herzberg & Gazel, 2009; Hole, 2015), well below anomalously high temperatures
181 calculated for the likely plume-related Deccan and Siberian LIPs, but at least 100 °C higher than
182 normal ambient upper mantle (Herzberg & Gazel, 2009; Sobolev et al., 2011). These moderately
183 high temperatures raise questions about the origins of that heat in the absence of a mantle plume;
184 one possibility is continental insulation beneath supercontinents (e.g., Coltice et al., 2007; Rey,
185 2015). Within this framework, the wide geochemical variability observed in ENA tholeiitic dikes
186 and sills makes it a particularly good focus region for placing new geochemical constraints on
187 the diversity of magma source origins and the process of continental flood basalt production
188 during rifting.

189 **2. METHODS**

190 **2.1. CAMP sample selection and preparation**

191 Tholeiitic basalt and diabase samples were selected to achieve a representative coverage across
192 the geochemical variability observed in trace elements and Sr-Nd-Pb isotopes for the southern
193 ENA region (12 samples), as well as targeted comparison to other regions within CAMP
194 including the northern ENA Newark basin (six samples), Sierra Leone (one sample), and
195 Morocco (one sample) (Table 1, Figure 1). The selected samples had relatively fresh, unaltered
196 appearances, with prior major and trace element results indicative of minimal crustal assimilation
197 or post-eruptive alteration (Callegaro et al., 2013, 2017; Marzoli et al., 2019; Merle et al., 2014).
198 Of these, two southern ENA samples (CS28 and CS57) were selected because they are
199 particularly Mg-rich (> 12 wt.% MgO) and are among the most primitive rocks ever recovered
200 from CAMP (Table 1; Callegaro et al., 2013). An exception to the above criteria is sample
201 NEW68 from the Preakness unit of the Newark Basin, which was selected because it is likely
202 crustally contaminated (Merle et al., 2014).

203 The samples analyzed for this study were all collected during prior research, and sampling
204 locations and previous geochemical measurements have been published elsewhere (Callegaro et
205 al., 2013, 2017; Marzoli et al., 2019; Merle et al., 2014) (Table 1). Prior to analysis for the
206 current study, any weathered rinds were removed by cutting with a trim saw. Fresh, visibly
207 unaltered material was then broken into finer pieces using a rock hammer, which was protected
208 with layers of clean plastic sheeting to prevent contamination. Sample material was then reduced
209 to small chips and powdered using an agate mortar and pestle. Larger samples with a sufficient
210 volume of material were further powdered using a Spex Shatterbox alumina grinding apparatus.
211 Samples were prepared in this manner either at the University of Padova or at the University of
212 Nebraska-Lincoln.

213 **2.2. Analytical methods**

214 Samples were analyzed for Hf isotopes in the Center for Elemental Mass Spectrometry, School
215 of Earth, Ocean, and Environment, University of South Carolina. An aliquot of 100 mg of rock
216 powder was weighed and digested in a Teflon-distilled HF:HNO₃ mixture in a 3:1 ratio. After
217 dissolution, the solution was dried repeatedly in 6N HCl, after which Hf was separated from
218 matrix elements using Eichrom LN-Spec Resin and methods after Munker et al. (2001). Hafnium
219 separates were analyzed by mass spectrometry methods using a Thermo Neptune multi-collector
220 inductively-coupled plasma mass spectrometer (MC-ICP-MS). Procedural blanks recorded Hf
221 concentrations under 50 pg, and analytical precision was within 0.0017% (2σ standard error) for
222 all measured samples (Table 2). Isotope compositions were corrected for mass fractionation
223 using $^{179}\text{Hf}/^{177}\text{Hf} = 0.7325$. The JMC-475 standard was determined to have $^{176}\text{Hf}/^{177}\text{Hf} =$
224 0.282152 ± 0.000004 (n = 10) for the first round of analyses and $^{176}\text{Hf}/^{177}\text{Hf} = 0.282142 \pm$
225 0.000007 (n = 10) for the second batch (Table 2). The data were corrected for instrumental bias
226 using a JMC-475 reference value of 0.282160. As an additional test of external reproducibility,
227 we analyzed a gabbroic sample from the Freetown Layered Complex (Sierra Leone) as a
228 replicate of an earlier measurement by Callegaro et al. (2017), using a separate dissolution. Our
229 newly measured $^{176}\text{Hf}/^{177}\text{Hf}$ ratio for this sample (0.282917 ± 0.000005 ; Table 2) is similar to the
230 prior published result (0.282937 ± 0.000012). The two results are slightly outside of 2σ
231 uncertainty with each other, however, which may be attributed to minor sample heterogeneity
232 and the measurement of separate sample dissolutions. Additional analytical details and standard
233 information can be found in Khanna et al. (2014), Mallick et al. (2015), and Frisby et al. (2016).

234 3. RESULTS

235 All data measured in this study have been age corrected to a crystallization age of 201 Ma using
236 Lu/Hf ratios previously published for these samples (Callegaro et al., 2013, 2017; Marzoli et al.,
237 2019; Merle et al., 2014) (Table 2); age-corrected isotopic ratios are hereafter indicated with
238 “201 Ma” notation. A conservative uncertainty of ~5% for the Lu/Hf ratio translates to less than
239 0.3 ϵ_{Hf} units of uncertainty in the initial isotopic composition for rocks of this age, and has no
240 effect on the conclusions of this study. Most samples from the southern ENA region form a
241 distinct array exhibiting a shallower slope (slope = 0.92 ± 0.12) than the terrestrial array
242 (Vervoort et al., 2011), being slightly shifted toward higher $\epsilon_{\text{Hf } 201\text{Ma}}$ ratios for a given $\epsilon_{\text{Nd } 201\text{Ma}}$
243 value (Table 2, Figure 2a). A notable exception is sample CS73 from Virginia, which plots along
244 the terrestrial array. The oblique trend relative to the terrestrial array defined by southern ENA
245 samples resembles trends previously observed for basalts from Hawaii (Blichert-Toft et al.,
246 1999; Salters et al., 2006) and the Karoo LIP (Jourdan et al., 2007) (Figure 2a). Southern ENA
247 $\epsilon_{\text{Hf } 201\text{Ma}}$ ratios also form a slightly positive correlation with $^{206}\text{Pb}/^{204}\text{Pb}_{201\text{Ma}}$ isotope ratios
248 (Callegaro et al., 2013) (Figure 2b). The latitudinal $\epsilon_{\text{Hf } 201\text{Ma}}$ profile between 34 and 37 °N shows
249 a decreasing southward gradient (Figure S1) toward more enriched (less radiogenic) isotope
250 ratios, with the exception of sample CS73.

251 In contrast with ENA samples, those from the Newark basin, Morocco, and Sierra Leone are
252 overall consistent with the global array (Vervoort et al., 2011) (Figure 2a). An exception is the
253 sample NEW68, a Preakness unit tholeiite selected for comparison due to its distinct
254 geochemical signature indicative of crustal assimilation (Merle et al., 2014); NEW68 has a
255 slightly higher $\epsilon_{\text{Hf } 201\text{Ma}}$ ratio for its $\epsilon_{\text{Nd } 201\text{Ma}}$ than other Newark basin basalts. Newark basin
256 samples exhibit a range of $\epsilon_{\text{Hf } 201\text{Ma}}$ values from ~0 to +5 (Figure S1).

257 4. DISCUSSION

258 The shallow slope of southern ENA tholeiites relative to the terrestrial array (Figure 2a, Table 2)
259 indicates a systematically increasing contribution from a low- ϵ_{Hf} source towards the south
260 (Figure S1). However, unlike previous data sets such as Hawaiian basalts (Blichert-Toft et al.,
261 1999; Salters et al., 2006) and the Karoo LIP (Jourdan et al., 2007), the southern ENA CAMP
262 array extends towards low $^{206}\text{Pb}/^{204}\text{Pb}_{201\text{Ma}}$ ratios at the low- $\epsilon_{\text{Nd } 201\text{Ma}}$ end of the array. Below, we
263 explore a series of melt mixing and assimilation scenarios and compare the outcomes to the
264 observed CAMP trace element and isotopic data, in an attempt to explain the origins of these
265 isotopic characteristics.

266 4.1. Crustal assimilation in Carolina tholeiites

267 As noted above, aside from a few samples, recent isotopic studies of ENA and other CAMP
268 rocks have indicated relatively minor crustal assimilation effects (up to 10% assimilation) in
269 ENA tholeiites (Callegaro et al., 2013; Merle et al., 2014; Whalen et al., 2015), which have
270 relatively low age-corrected $^{187}\text{Os}/^{188}\text{Os}_{201\text{Ma}}$ (0.128 – 0.187, mean 0.137) despite high
271 $^{87}\text{Sr}/^{86}\text{Sr}_{201\text{Ma}}$ (0.70438 - 0.71074, mean 0.70613), high $^{207}\text{Pb}/^{204}\text{Pb}_{201\text{Ma}}$ (15.54 - 15.67, mean
272 15.61), variable $^{206}\text{Pb}/^{204}\text{Pb}_{201\text{Ma}}$ (17.41 - 18.65, mean 18.23), and low $^{143}\text{Nd}/^{144}\text{Nd}_{201\text{Ma}}$ ratios
273 (0.51204 - 0.51251, mean 0.51230). However, due to a lack of Hf compositional and isotopic
274 data for the potential end-member continental assimilants in the ENA province, it is unclear what
275 effects up to 10% crustal assimilation may have had on the Hf isotope compositions of ENA
276 CAMP magmas. To evaluate the potential impacts of assimilation on the Hf data set, we
277 calculated the effects of assimilation-fractional crystallization on ENA basalts using energy-
278 constrained methods after Bohron and Spera (2001) and Spera and Bohron (2001) (Tables S1,

279 S2; Figure 3), and considering three potential assimilants: local upper continental crust, and both
280 mafic and intermediate-SiO₂, lower crustal granulite rocks. To simplify the scenarios tested, we
281 make several initial assumptions, including the temperatures, compositions, and energy
282 properties of the primary magma and three assimilants (see Tables S1, S2). Our calculations also
283 assume a primary magma composition resembling the most incompatible element-depleted,
284 southern ENA tholeiite measured in this study with respect to Hf (sample CS49, with low [Hf] =
285 1.3 ppm, high $\epsilon_{\text{Hf } 201\text{Ma}} = +5.86$) (Table 2).

286 To estimate the average composition of local upper continental crust, we used the mean
287 compositions of measured Carolina terrane crustal rocks from Pettingill et al. (1984) and Sinha et
288 al. (1996) and the data compilation of Whalen et al. (2015) (Table S1). The composition and age
289 of the lower basement of the Carolina terrane is less well-constrained. In general, while some
290 lower continental crust (LCC) may be Phanerozoic in age, most LCC worldwide is likely
291 composed of Archean to Proterozoic Precambrian granulites with a range of mafic to felsic
292 compositions (e.g., Huang et al., 1995; Schmitz et al., 2004; Vervoort et al., 2000). Most lower
293 crustal granulites measured lie along the terrestrial $\epsilon_{\text{Nd}} - \epsilon_{\text{Hf}}$ array (Vervoort et al., 2000), but
294 some granulite xenoliths exhibit decoupling of ϵ_{Hf} from ϵ_{Nd} , likely caused by the presence of
295 cumulate or restite igneous minerals or by fractionation during metamorphic mineral growth
296 (Schmitz et al., 2004). The decoupling toward higher ϵ_{Hf} relative to the terrestrial array is
297 primarily observed in Proterozoic granulites (Huang et al., 1995; Schmitz et al., 2004; Zartman et
298 al., 2013), and so may play a role as there is isotopic evidence that local Carolina terrane LCC is
299 dominantly Proterozoic in age (Ingle et al., 2003). As for major element compositions, while
300 much of the LCC may be mafic, Zhao and Guo (2019) and Guo et al. (2019) have observed that
301 local Carolina LCC likely has an overall intermediate SiO₂ content; we thus test both mafic and

302 intermediate-SiO₂ LCC compositions (Figure 3, Table S1). The mafic LCC composition used
303 here resembles mafic granulite xenoliths from Michigan (Zartman et al., 2013) with decoupled
304 ϵ_{Hf} and ϵ_{Nd} ; alternative assimilation trajectories for mafic granulites lying along the terrestrial
305 array exhibited a poorer fit and, for simplicity, are not shown. We assume that the intermediate
306 granulite has comparatively enriched (unradiogenic) Hf and Nd isotopes and resembles
307 intermediate-SiO₂ granulite xenoliths from South Africa and measured by Schmitz et al. (2004)
308 (Table S1). Several Pb isotopic compositions were tested for the LCC assimilation scenarios to
309 determine the best fit to the measured ENA CAMP data set (see Figure 3, Table S1, S2),
310 considering the large span of Pb isotopic ratios exhibited by the basement terranes previously
311 accreted to ENA (Pettingill et al., 1984; Sinha et al., 1996; Whalen et al., 2015). Because well-
312 characterized intermediate-SiO₂ granulite xenoliths in the literature are largely peraluminous, a
313 composition that may not be representative of all lower crust, we further tested a more
314 aluminum-poor composition based on well-characterized, intermediate-SiO₂ granulites from
315 Jonsa, Finland (Nehring et al., 2010); however, the Finnish granulite composition likewise
316 exhibited a poorer fit than the other results, so for simplicity it is not shown.

317 We show our calculated crustal assimilation trajectories in Figure 3. Only the relatively enriched,
318 intermediate-SiO₂ granulite assimilant can account for most of the Hf-Nd isotopic variability
319 observed in our samples with 10% assimilation or less (Figure 3). Up to 10% assimilation of
320 Carolina terrane UCC rocks cannot explain most of the $\epsilon_{\text{Hf}}-\epsilon_{\text{Nd}}$ data array (Figure 3). Mafic LCC
321 assimilation trajectories deviate to much higher ϵ_{Hf} than our sample data (Figure 3) when using
322 the isotopically decoupled assimilant after Zartman et al. (2013), and none of the mafic granulite
323 Pb isotope compositions tested are able to explain our samples' Pb isotopes using only 10%
324 addition (see also Callegaro et al., 2013; Merle et al., 2014; Whalen et al., 2015). For

325 intermediate-SiO₂ LCC, the Pb isotope composition of an assimilant needs to be relatively
326 unradiogenic (e.g., ²⁰⁶Pb/²⁰⁴Pb ~17.0-17.3), but the assimilant must also have relatively
327 unradiogenic ¹⁷⁶Hf/¹⁷⁷Hf and ¹⁴³Nd/¹⁴⁴Nd compositions (Figure 3). Such a low ²⁰⁶Pb/²⁰⁴Pb
328 composition may be plausible when compared with the ranges measured in granulites from
329 Antarctica (Wyszczanski et al., 1995), Scotland (Halliday et al., 1993), and Michigan (Zartman
330 et al., 2013), which provide global examples of intermediate to felsic lower crustal granulites,
331 and also in light of the low ²⁰⁶Pb/²⁰⁴Pb signatures observed in some exposed Carolina terrane
332 rocks (granulites, charnockites, and anorthosites; Sinha et al., 1996).

333 All of our LCC assimilation calculations exhibit concave-down curvature in Figure 3, suggesting
334 that, e.g., Pb may generally be more significantly impacted than Hf by assimilation processes
335 because of its higher concentrations in granulitic basement relative to mantle-derived basalts
336 (e.g., Zartman et al., 2013). We further note that among our tested compositions, only a crustal
337 contaminant containing accessory zircon, like our intermediate-SiO₂ granulite composition, had
338 sufficiently high Hf partition coefficients to reproduce the isotope compositions observed in our
339 southern ENA data set with only 10% assimilation. In our calculations, the presence of minor
340 zircon in the assimilant rock also extends the compositions of magmas experiencing even minor
341 assimilation to more highly unradiogenic ε_{Hf} values (Figure 3). The role of accessory minerals in
342 magma assimilation processes is, however, presently unclear and likely to be more complex than
343 our models allow. For example, minerals like zircon may be effectively dissolved from country
344 rocks adjacent to mafic sills and dikes early in the melt-rock interaction process, depending on
345 local zircon abundance, grain size, and Zr saturation in the melt (e.g., Bindeman & Melnik,
346 2016). Melt-rock interaction between intruding magmas and granulitic country rocks is also
347 likely to be highly variable both spatially and over time, beyond the relatively simple calculated

348 scenarios shown in Figure 3. We thus only conclude that limited absorption of intermediate-
349 SiO₂, relatively isotopically enriched granulitic wallrock by primary CAMP tholeiitic magmas
350 may in part account for elevation of southern ENA samples above the terrestrial data array,
351 within the 10% assimilation constraint previously identified using Os isotopes (Callegaro et al.,
352 2013; Merle et al., 2014).

353 **4.2. Source origins of Eastern North American tholeiites**

354 While assimilation of crust may play a role in generating part of the isotopic variability observed,
355 mantle source heterogeneity is still required to fully explain the origins of ENA CAMP
356 (Callegaro et al., 2013; Merle et al., 2014; Whalen et al., 2015). Based on their distribution,
357 much of the isotopic variations observed in ENA CAMP tholeiite samples may require the
358 involvement of multiple distinct mantle sources (Figure 2). Below we explore current working
359 hypotheses for heterogeneous source origins of the southern ENA CAMP data set, including 1)
360 global mantle reservoirs, 2) SCLM, and 3) recently recycled crust in the local asthenosphere.

361 *4.2.1. Hypothesis 1: Global mantle reservoirs as a source for CAMP*

362 A technique for identifying possible plume-derived and/or long-lived mantle reservoirs for the
363 central Atlantic region is considering the end member basalt compositions observed in local
364 ocean island basalts, such as the Azores (Béguelin et al., 2017), Madeira (Geldmacher et al.,
365 2011), or Bermuda (Mazza et al., 2019), as well as Mesozoic MORB (Janney & Castillo, 2001)
366 and recently identified Eocene magmatism in the Appalachians (Mazza et al., 2017) (Figure 2).
367 However, prior research (e.g., Marzoli et al., 2019, and references therein) has consistently
368 shown that such end-members cannot explain all of the isotopic compositions observed in

369 CAMP, and indeed Atlantic intraplate basalts span a notably different compositional range than
370 that observed across the ENA CAMP data set.

371 Long-lived mantle components, such as depleted MORB mantle (DMM) and the most extreme
372 enriched mantle end-members (EM-1 and EM-2), define a broader range of isotopic
373 compositions, and their potential contribution in generating the observed trends in CAMP
374 compositions is examined here. This scenario resembles the proposed origin for many hotspot
375 volcanic centers and ocean islands, and would potentially suggest the presence in the melt zone
376 of materials transported from the deep mantle via a mantle plume. However, recent isotope
377 measurements of ENA CAMP have demonstrated that mixing of long-lived, global mantle
378 components in a heterogeneous mantle source is unable to fully explain the range of isotope
379 compositions observed, particularly for Pb isotope ratios (Callegaro et al., 2013, 2014, 2017;
380 Merle et al., 2011, 2014), and that outcome remains unchanged by our new Hf contributions as
381 demonstrated by our mixing calculations (Figures S2, S3). In those calculations, we test more
382 recent estimates for the isotopic compositions of EM-1 and EM-2 (e.g., Jackson and Dasgupta,
383 2008; Jackson et al., 2007; Table S1), which have less extreme Pb isotope compositions than,
384 e.g., earlier estimates that were used in prior CAMP studies (e.g., Whalen et al., 2015); our
385 results do not, however, achieve a better fit to ENA CAMP isotopic data than previous work. We
386 further note that while parts of our data set resemble partial melts of enriched mantle reservoirs
387 like EM-1 or EM-2, the trend of the southern ENA CAMP data array is inconsistent with the
388 sense of enrichment implied by mixing trajectories in Figures S2 and S3. In particular, the
389 samples with isotopic signatures towards the low- ϵ_{Hf} end of the data array (i.e., trending towards
390 enriched mantle) also exhibit relatively low Pb isotope ratios and thus appear to trend away from

391 the same end members in Pb-isotope space. This apparent mismatch indicates that additional
392 partial melt sources must be considered to fully explain the origins of southern ENA CAMP.

393 *4.2.2. Hypothesis 2: Melting of subcontinental lithospheric mantle*

394 It is possible that the lithospheric mantle beneath CAMP has experienced prior melting (e.g.,
395 during rifting of Laurussia) that may have left a depleted and refractory lithospheric mantle
396 residue. The moderately high temperatures calculated for CAMP (Herzberg & Gazel, 2009) may
397 have then been sufficient to cause melting of the refractory SCLM: at temperatures of 1480°C
398 and relatively low mantle pressures (1.5-2.0 GPa), Falloon and Danyushevsky (2000) predicted
399 6-12% melting of anhydrous harzburgite. This refractory mantle should be depleted in
400 incompatible trace elements and thus may resemble depleted asthenospheric mantle in trace
401 element and isotopic composition, making it difficult to uniquely identify. We note that in this
402 scenario, heating and melting of refractory lithosphere would need to be sufficiently widespread
403 to explain the large volume of magma likely deposited during CAMP. The total volume
404 emplaced remains unknown, but the province spans a total area of approximately 10^7 km², as
405 noted above. We further note that mantle temperatures sufficient to remelt refractory SCLM are
406 also sufficient to melt the more fertile underlying lherzolitic asthenosphere, and the geochemical
407 signatures of these two scenarios are expected to significantly overlap. Such asthenospheric
408 melting is likely to produce an additional volume of magma that would overwhelm the trace
409 element contribution from the less fertile, trace element depleted, harzburgitic lithospheric rocks.

410 On the other hand, supra-subduction zone SCLM, such as that produced during the assembly of
411 Pangea, is further expected to be variably infiltrated by metasomatic fluids that would impart a
412 more enriched trace element and isotopic composition. A metasomatized SCLM is thus an

413 alternative and more fertile melt source that has been suggested for CAMP tholeiites (e.g.,
414 Alibert, 1985; Bertrand, 1991; Bertrand et al., 1982; Cebriá et al., 2003; De Min et al., 2003;
415 Deckart et al., 2005; Dostal & Durning, 1998; Dupuy et al., 1988; Heatherington & Mueller,
416 1999; Jourdan et al., 2003; Marsh, 1987; Merle et al., 2011; Pegram, 1990; Puffer, 1992; Puffer,
417 2003), including high-TiO₂ CAMP magmas from Sierra Leone (Callegaro et al., 2017). In Sierra
418 Leone, high-TiO₂ gabbros of the Freetown Layered Complex exhibit an enriched isotopic
419 signature characterized by very high ²⁰⁷Pb/²⁰⁴Pb_{201Ma} ratios but low ²⁰⁶Pb/²⁰⁴Pb_{201Ma} (Figure 2). A
420 small amount of lamproite magma, inferred to derive from a local, subduction-metasomatized
421 SCLM source, was tested as a plausible contributor, mixed with a dominant asthenospheric melt
422 (Callegaro et al., 2017). A group of high-TiO₂ samples from Brazil (Merle et al., 2011) with
423 comparatively low ²⁰⁷Pb/²⁰⁶Pb (Figure 2) may also sample a distinct, localized mantle or SCLM
424 source (Merle et al., 2011). While some southern ENA CAMP rocks share similar (if less
425 extreme) Pb isotopic signatures to Sierra Leone gabbros (Figure 2), they are otherwise quite
426 different, having low TiO₂ contents, higher ⁸⁷Sr/⁸⁶Sr_{201Ma}, and lower ¹⁴³Nd/¹⁴⁴Nd_{201Ma} than the
427 Freetown gabbros.

428 Without local volcanic samples inferred to derive from SCLM melt sources, or SCLM-derived
429 local xenoliths for comparison, there are no regional Hf isotopic constraints for southern ENA
430 SCLM, making it difficult to directly test for SCLM melt contributions to southern ENA CAMP
431 basalts. Eastern North American CAMP was located farther from cratonic or peri-cratonic
432 settings than magmas from Brazil or Sierra Leone, though, suggesting SCLM is a less likely melt
433 source for ENA. We further note that although there are rare exceptions (e.g., Griffin et al.,
434 2000), global SCLM xenolith data largely have ε_{Hf} > +9 (Choi et al., 2008, 2010; Shaw et al.,
435 2007; Wittig et al., 2007, 2010) (Figure S4), making it difficult to explain the observed array

436 primarily by this mechanism. We cannot completely rule out an exotic, metasomatized
437 lithospheric mantle melt component influencing the composition of individual samples with
438 slightly elevated ϵ_{Hf} (Figure 2a), but based on prior work, we consider it an unlikely overall melt
439 source for low-TiO₂ LIP tholeiites.

440 *4.2.3. Hypothesis 3: Paleozoic crustal recycling in the asthenosphere beneath CAMP*

441 In a third scenario, we explore Paleozoic recycling of crustal material and production of a
442 modified mantle source beneath ENA, which is subsequently melted during the CAMP event.
443 Callegaro et al. (2013) suggested that ENA magmas may derive from direct melting of local
444 asthenosphere containing 1) depleted upper mantle, 2) recycled upper continental crustal rocks,
445 possibly as subducted Paleozoic terrigenous sediments associated with the assembly of Pangea,
446 and 3) lower continental crustal rocks, perhaps delaminated and locally reintroduced into the
447 convecting melt region (see e.g., Magni and Király, 2019). Whalen et al. (2015) suggested a
448 related scenario in which melts and/or aqueous fluids derived from subducted sediments
449 modified the local mantle melt source beneath ENA, with a stronger fluid-derived signature in
450 the south and more melt metasomatism recorded to the north. Below, we explore the constraints
451 that Hf isotopes would place on both models, and attempt to evaluate the possible role of
452 recently recycled crust in ENA CAMP magma generation.

453 *4.2.3.1. Paleozoic recycling of upper and lower continental crust.* Crustal recycling provides
454 possible explanations for an incompatible-element enriched source with notably high Lu/Hf
455 ratios, as implied by the radiogenic $\epsilon_{\text{Hf } 201\text{Ma}}$ relative to $\epsilon_{\text{Nd } 201\text{Ma}}$ observed in southern ENA
456 CAMP. As an initial test of melting a recently subduction-modified mantle source, we first
457 consider whether direct mixing of local depleted asthenospheric mantle melts with recycled

458 upper and local crust, i.e. the scenario suggested by Callegaro et al. (2013), can directly produce
459 the observed data array (Figure 4). As discussed above, most continental crustal rocks plot along
460 the terrestrial array, making it difficult to reproduce the southern ENA data trend. However,
461 some lower crustal mafic granulites may inherit a high, decoupled ϵ_{Hf} ratio due to the presence of
462 significantly old garnet with high Lu/Hf ratios (e.g., Blichert-Toft et al., 2005), similar to some
463 of the xenoliths measured by Zartman et al. (2013). If recycled, e.g., by delamination into the
464 asthenosphere, mafic LCC thus represents a plausible mantle source with elevated ϵ_{Hf} above the
465 mantle array in Figure 2a. However, an additional unradiogenic (enriched) Hf source lying closer
466 to the mantle array would then also be required to fully explain the observed ENA data. Upper
467 continental crust is typically more enriched in incompatible elements and should plot along the
468 mantle array (Table S1, Figure 2a), making it a reasonable, additional recycled source and
469 possibly lending support to the suggested model of Callegaro et al. (2013). Upper crustal
470 material could have been introduced to the regional mantle by subduction of terrigenous marine
471 sediments; if local sediment deposition occurred near a subducting margin and was relatively
472 close to a weathering continental source, such sediments would closely resemble the average
473 composition of nearby continental terranes, as modeled by Callegaro et al. (2013).

474 However, we observe that direct mixing of melts from ambient asthenosphere with a typical DM
475 isotopic composition (Salters and Stracke, 2004; Workman and Hart, 2005) with recycled LCC
476 and UCC material is unable to explain the Hf and Pb isotopes measured for southern ENA
477 CAMP, at least within currently available constraints (e.g., Figure 2b). This is illustrated by the
478 isotopic compositions of the suggested end-members in Table S1 and Figure 2b, where we
479 identify a Proterozoic lower crustal end-member represented by mafic granulite Michigan
480 xenoliths (“Mafic LCC,” Zartman et al., 2013), an upper crust end-member represented by local

481 average Carolina terrane (“UCC”) ($^{206}\text{Pb}/^{204}\text{Pb}$ ranges between ca. 17.1 and 17.5 for Carolina
482 terrane rocks; Pettingill et al., 1984; Sinha et al., 1996), and ambient mantle modeled as a DM
483 component (“DMM”). In particular, crustal components with ϵ_{Hf} and ϵ_{Nd} values capable of
484 explaining the CAMP array do not span a sufficiently large range in Pb isotopic compositions to
485 explain the measured data (Figure 2).

486 *4.2.3.2. Paleozoic recycling and metasomatism of the asthenosphere.* Alternatively, Whalen et al.
487 (2015) suggested a scenario for the recycling of regional Paleozoic upper crustal sediments into
488 the subcontinental asthenosphere without invoking lower crustal delamination. By incorporating
489 subducted pelagic marine sediments, this scenario offers an alternative to recycled local UCC
490 from the Carolina terrane, one that notably plots above the mantle array; such a component may
491 thus alleviate the need for melting of exotic (i.e., with decoupled ϵ_{Hf} and ϵ_{Nd}) mafic Proterozoic
492 LCC rocks. Unlike our upper crust estimate for the Carolina terrane, weathered terrigenous
493 marine sediments have elevated Lu/Hf ratios due to the progressive removal of heavy detritus
494 minerals like zircon during continental weathering and differential river transport; the elevated
495 Lu/Hf ultimately produces high ϵ_{Hf} relative to ϵ_{Nd} in clay-rich marine pelagic sediments (Chauvel
496 et al., 2014; Garcon et al., 2013, 2014; Vervoort et al., 1999, 2011). Chauvel et al. (2008)
497 determined time-averaged ϵ_{Hf} and ϵ_{Nd} isotope compositions for typical subducted sediments,
498 which reside in the same part of the Hf-Nd isotope diagram as both marine Fe-Mn precipitates
499 and seawater (e.g., Albarede et al., 1998) (Figure 2a). As an alternative to the prior mixing
500 scenario with upper and lower continental crust, here we test mixing of partial melts of depleted
501 asthenosphere with a combination of 1) local Carolina terrane crust and 2) global average marine
502 sediments (GLOSS, after Plank and Langmuir (1998) and Chauvel et al. (2008); Table S1).
503 Specifically, we tested a Paleozoic marine sediment source subducted beneath the CAMP

504 province during the construction of Pangea at ~370 Ma, i.e., 170 Ma prior to the CAMP melting
505 event, after Merle et al. (2014), Callegaro et al. (2013), and Whalen et al. (2015).

506 In Figure 4a, where mixing results are reported along with our data, ternary mixing of depleted
507 mantle, Carolina UCC crust, and average global sediment cannot account for the Hf-Nd isotopic
508 variability observed in ENA samples. While trace element concentrations in recycled sources are
509 necessarily averages of heterogeneous materials, and a small change in the trace element budget
510 of upper crust, for example, may appear to resolve the observed discrepancy in mixing
511 trajectories, the end members themselves are also inconsistent. Average global subducted
512 sediment has elevated ϵ_{Hf} relative to ϵ_{Nd} , similar to the southern ENA data array (e.g., Chauvel et
513 al., 2008; Chen et al., 2013; Vervoort et al., 2011), but its highly radiogenic Pb isotope ratios are
514 inconsistent with our most extreme samples, which have the lowest $\epsilon_{\text{Nd } 201\text{Ma}}$ but also the least
515 radiogenic $^{206}\text{Pb}/^{204}\text{Pb}_{201\text{Ma}}$ and $^{207}\text{Pb}/^{204}\text{Pb}_{201\text{Ma}}$. While contributions of melts from recycled
516 crustal rocks could thus explain some of the intermediate compositions observed in the ENA
517 CAMP data set, the scenario is a poor explanation for the most unradiogenic samples with
518 respect to $\epsilon_{\text{Hf } 201\text{Ma}}$.

519 A more plausible recycling hypothesis is the creation of a hybrid, metasomatised mantle source
520 by the addition of subduction-derived fluids to the peridotitic mantle wedge, which in turn
521 partially melts to produce local CAMP tholeiites. Whalen et al. (2015) suggested that the
522 subducted sediments in the subcontinental CAMP asthenosphere have dehydrated and/or melted,
523 producing fluids that metasomatically modified ambient peridotite. They further tied the nature
524 of the metasomatic fluid (aqueous fluid in the south vs. silicate melt in the north) to geographic
525 variations along the ENA subprovince as noted above.

526 Hafnium is primarily considered a tracer of melt and not aqueous fluid metasomatism in modern
527 arc environments (e.g., Kempton et al., 2018), because Hf is expected to have relatively low
528 aqueous solubility (e.g., Banks, 1950; Linnen, 1998). However, the relatively low fluid mobility
529 of Hf means dehydration of subducted sediments may produce a relatively high Lu/Hf
530 metasomatic fluid, such that a modified mantle may develop relatively high ϵ_{Hf} ratios over time
531 (e.g., Janney et al., 2005; Kempton et al., 2018). If northern ENA tholeiites record primarily melt
532 metasomatism while southern ENA tholeiites record ancient fluid metasomatism of the regional
533 mantle source, as posited by Whalen et al. (2015), southern ENA mantle could then have
534 developed variably high ϵ_{Hf} compared to ϵ_{Nd} , while northern ENA mantle did not, similar to our
535 observations; however, such a difference in fluid vs. melt metasomatic effects could be
536 confounded by other factors. For instance, subducted metasediments may include stable
537 metamorphic garnet, which could impact the Lu/Hf ratio of metasomatizing melts or fluids
538 derived from the subducted rocks (e.g., Kempton et al., 2018). Some lithospheric mantle
539 xenoliths that have experienced metasomatism also have extreme high ϵ_{Hf} ratios, unlike ENA
540 CAMP basalts (e.g., Armytage et al., 2015). The impact of metasomatic source effects on long-
541 term $^{176}\text{Hf}/^{177}\text{Hf}$ ratios is thus unclear and warrants more careful analysis.

542 Here we introduce a new model for calculating the trace element and isotope compositions of
543 both subduction-modified depleted mantle wedge and subsequent partial melts of that modified
544 mantle source (Table S4). In the model, three initial reservoirs are age-corrected to the time of
545 subduction recycling: 1) ambient peridotite asthenosphere after Salters and Stracke's (2004)
546 Depleted Mantle; 2) average global oceanic sediment similar to GLOSS (Chauvel et al., 2008;
547 Plank and Langmuir, 1998); and 3) altered oceanic crust (AOC) calculated from Atlantic drill
548 core compositions (Staudigel et al., 1996). The composition of a metasomatizing fluid is then

549 determined for a range of mixtures of 1) an AOC-derived aqueous fluid and 2) either a melt or an
550 aqueous fluid derived from subducted sediment. Trace element concentrations in all AOC and
551 sediment-derived fluids are calculated using mobility and partition coefficients after Kogiso et al.
552 (1997), Stracke et al. (2003), and Johnson and Plank (2000) (Table S3; see Supporting
553 Information). The composition of the modified wedge is then determined for 0-10% fluid
554 addition to the mantle, and across the full range of fluid mixtures. Next, the resulting modified
555 mantle composition is tracked for isotopic decay from the time of recycling and metasomatism
556 (370 Ma) until the time of melting (201 Ma) to determine the isotopic and trace element
557 compositions of the mantle during CAMP. Predicted trace element compositions in CAMP
558 basalts were determined using a simple modal batch melting model and melt fraction of 6%, with
559 garnet lherzolite mineral/melt partition coefficients and residual peridotite modes as in Table S3.

560 Results from the wedge metasomatism and melting model, shown in Figure 5, approach or
561 overlap with the most isotopically depleted southern ENA CAMP basalt composition (sample
562 CS49), as long as the subduction and recycling age is relatively young. The results shown in
563 Figure 5 assume a Paleozoic subduction age of 370 Ma, i.e. the recycling age previously
564 suggested by Merle et al. (2014), Callegaro et al. (2013), and Whalen et al. (2015). Recycling
565 ages older than Paleozoic subduction fail to reproduce the $\epsilon_{\text{Hf}}^{201\text{Ma}}$, $\epsilon_{\text{Nd}}^{201\text{Ma}}$, and Pb isotope
566 ratios observed in our basalts. Melting of a mantle source modified by a purely aqueous
567 metasomatic fluid and dominated by sediment-derived fluid (i.e., the AOC-derived fluid \leq 25%
568 of the fluid mixture) can reasonably explain sample CS49 with less than 10% fluid addition,
569 although we note that the Pb isotope results shown in Figure 5c are close but not an exact fit to
570 the measured data at the lowest fluid addition values ($<$ 4%) that work best for ϵ_{Hf} and ϵ_{Nd}
571 isotopes.

572 We further note that for the most radiogenic Pb isotopes observed in ENA CAMP tholeiites,
573 mantle metasomatism dominated by aqueous fluid addition is a closer match than melt
574 metasomatism, even for some Newark basin samples (Figure 5c). This observation conflicts with
575 the suggestion of Whalen et al. (2015) that differences in Paleozoic subduction angles modified
576 the metasomatic regime from north to south beneath the North American margin, and that more
577 northerly ENA tholeiites were dominated by melt- and not aqueous fluid metasomatism of the
578 Paleozoic mantle. We would argue that while the exact proportions of fluid addition to the
579 mantle wedge may have been variable, a fluid-dominated metasomatic agent where most of the
580 fluid is derived from subducted sediments (i.e., only a limited proportion of the fluid is
581 contributed by AOC) provides a particularly good match to the radiogenic $^{206}\text{Pb}/^{204}\text{Pb}$ ENA end-
582 member (Figure 5).

583 *4.2.3.3. A hybrid recycling, metasomatism, and assimilation model for ENA CAMP.*

584 While the most primitive ENA CAMP magma analyzed here is in good agreement with
585 predictions for melting of metasomatized mantle, the remainder of our observed data array
586 cannot be explained purely by melting of such a source, even if the nature of that metasomatism
587 is itself regionally variable. Additional melting, mixing, and/or assimilation is thus required to
588 explain the full isotopic range exhibited by southern ENA CAMP. As explored above, the
589 compositions of southern ENA samples with low $\epsilon_{\text{Nd } 201\text{Ma}}$, comparatively radiogenic $\epsilon_{\text{Hf } 201\text{Ma}}$,
590 and relatively low $^{206}\text{Pb}/^{204}\text{Pb}_{201\text{Ma}}$ cannot be easily explained by melt mixing. Of the possible
591 sources considered here, only lower crustal granulites with decoupled Lu/Hf and Sm/Nd have the
592 necessary isotopic signatures to plausibly explain this composition, but the required proportional
593 contributions of melts from such a source are inconsistent in our calculations, and are too large
594 for some of the resulting mixtures to be basaltic in major element composition (Figure 6). Based

595 on the analysis above, we thus suggest that the ENA CAMP mantle melt source is dominated by
596 fluid-metasomatized asthenosphere, perhaps containing moderate quantities of recycled
597 continental crustal material, but not so much all of the observed data can be explained by direct
598 melting of those recycled rocks. Some minor (generally < 10%) assimilation of zircon-bearing,
599 intermediate-SiO₂, granulitic lower crust can then help to explain much of the southern ENA
600 data array (Figure 3). Our favored model thus includes a combination of factors, where some
601 direct melting of recycled crust is plausible, but minor crustal assimilation is also favored,
602 particularly to explain the southern ENA CAMP samples with the lowest $\epsilon_{\text{Hf } 201\text{Ma}}$ values. We
603 consider this a plausible model to explain the systematic trend towards low $\epsilon_{\text{Nd } 201\text{Ma}}$ and
604 $^{206}\text{Pb}/^{204}\text{Pb}_{201\text{Ma}}$ with comparatively high $\epsilon_{\text{Hf } 201\text{Ma}}$ and $^{207}\text{Pb}/^{204}\text{Pb}_{201\text{Ma}}$ in southern ENA basalts.

605 **4.3. Broader petrogenesis of Central Atlantic Magmatic Province tholeiites**

606 Figure 2a includes $^{176}\text{Hf}/^{177}\text{Hf}_{201\text{Ma}}$ results for magmas collected from other regions of CAMP,
607 including Sierra Leone and Morocco (Table 2). The range of isotopic compositions across
608 CAMP reflects localized processes, which for ENA include a local metasomatized mantle source
609 and minor assimilation of local crustal rocks. Such localized variations extend to other parts of
610 CAMP as well: samples from Sierra Leone, as noted above, exhibit notably high $\epsilon_{\text{Hf } 201\text{Ma}}$ values
611 for a given $^{206}\text{Pb}/^{204}\text{Pb}_{201\text{Ma}}$ ratio (Figure 2b) and have been suggested to incorporate melts from
612 local SCLM sources unique to that region, with an enriched composition comparable to
613 worldwide anorogenic lamproites, e.g. from Western Australia, Gaussberg, or Leucite Hills
614 (Callegaro et al., 2017). Likewise, in Pb isotope space, most magmas from CAMP form an array
615 with relatively high $^{207}\text{Pb}/^{204}\text{Pb}_{201\text{Ma}}$ for a given $^{206}\text{Pb}/^{204}\text{Pb}_{201\text{Ma}}$. High-TiO₂ samples from South
616 America have lower $^{207}\text{Pb}/^{204}\text{Pb}_{201\text{Ma}}$ for a given $^{206}\text{Pb}/^{204}\text{Pb}_{201\text{Ma}}$ (Figure 2) (Merle et al., 2011)

617 and may instead sample a localized mantle or SCLM source, as noted above (Deckart et al.,
618 2005; Merle et al., 2011). Central Atlantic Magmatic Province rocks from Guyana, Brazil, and
619 Sierra Leone also include high-TiO₂ tholeiites (TiO₂ > 2 wt. %). The high-TiO₂ CAMP magma
620 type, which exhibits very distinct isotopic signatures and trace element compositions (Marzoli et
621 al., 2018), is volumetrically minor and confined to a narrow belt bordering the Western African
622 Craton and the Amazonia Craton/Guyana Shield (De Min et al., 2003; Deckart et al., 2005;
623 Dupuy et al., 1988; Mauche et al., 1989).

624 The above observations indicate that a number of isotopic patterns are unique to specific regions
625 within CAMP and sample localized sources in the underlying mantle. The more geographically
626 restricted patterns do not clearly indicate a radially distributed hotspot-like signature that might
627 directly support mantle plume influence. Even if the arrival of a plume head was associated with
628 more widespread geographic dispersal and magma emplacement across broader terranes (e.g.,
629 McHone, 1996), making geographic emplacement patterns far from radial, such episodes should
630 follow a sequence where first SCLM is melted due to thermal erosion, and then upwelling
631 asthenospheric mantle melts (e.g., Ernst & Buchan, 2003; Ernst et al., 2001; Morgan, 1983).
632 Based on isotope measurements and age information, neither scenario (geographically radial
633 distribution of isotopic enrichment, or timing sequences indicative of large-scale lithospheric
634 erosion and melting followed by asthenospheric melting) appears clear for CAMP.

635 Instead, the more localized geographic patterns appear to support regional upwelling and melting
636 of local mantle, including localized melting of SCLM for some areas. Our observations could
637 thus plausibly be explained either 1) by a regional passive upwelling response to lithospheric
638 thinning, i.e., localized mantle convection response to rift initiation, or 2) by the arrival of a deep
639 upwelling mantle plume and accompanying melting of entrained local asthenosphere and, in

640 some areas, overlying lithosphere. A province-wide geochemical plume signature for CAMP
641 thus remains ambiguous.

642 **5. CONCLUSIONS**

643 Eastern North American CAMP basalts were plausibly generated by melting of regionally
644 upwelling, depleted upper mantle asthenosphere, which was likely metasomatized by aqueous
645 fluids derived from subducted oceanic crust and marine sediments. That melting may have been
646 accompanied by direct melting of relatively minor quantities of previously recycled (e.g.,
647 subducted or delaminated) crustal rocks. Melting was likely then followed by assimilation of
648 lower continental crust, possibly intermediate-SiO₂ granulites containing minor accessory
649 minerals like zircon, which may influence the hafnium isotopic compositions of the basalts. The
650 isotopic compositions of CAMP basalts do not directly support dominantly OIB-like, long-lived,
651 enriched mantle source reservoir origins, but instead vary with local upper mantle and
652 lithospheric compositions across the province, recording broad, regional mantle upwelling and
653 entrainment of local asthenosphere. Our findings thus suggest that continental rifting and the
654 generation and emplacement of the CAMP flood basalt province are best explained by regional
655 asthenospheric decompression beneath the Pangea supercontinent, neither requiring nor
656 definitively precluding the influence of a deep-seated mantle plume on continental rifting.

657 **Acknowledgments**

658 We thank Jörg Geldmacher and three anonymous reviewers for providing thoughtful suggestions
659 that helped improve a prior version of this manuscript. We also thank John Lassiter and Steve
660 Shirey for productive discussions about CAMP. Daren Blythe and Nathan Sorsen assisted with
661 sample preparation at UNL. L. Elkins acknowledges support from a UNL College of Arts and

662 Sciences International Collaboration Award that funded this research. Field sampling was
663 supported by the following grants: CARIPARO (Eccellenza 2008), PRIN (PRIN 20158A9CBM),
664 Padova University (CPDA132295/13) to A. M. N. Youbi (Caddi Ayyad University, Marrakech,
665 Morocco), H. Bertrand (ENS-Lyon, France), G. Bellieni (Padova University, Italy), S. Howard
666 (South Carolina Survey), and M. Higgins (North Carolina Survey) are kindly thanked for help
667 during fieldwork. Supporting data files are available at the IEDA data repository
668 (<https://doi.org/10.1594/IEDA/111347>).

669 REFERENCES

670 Albarede, F., A. Simonetti, J. D. Vervoort, J. Blichert-Toft, and W. Abouchami (1998), A Hf-Nd
671 isotopic correlation in ferromanganese nodules, *Geophysical Research Letters*, 25(20), 3895-
672 3898.

673 Alibert, C. (1985), A Sr-Nd isotope and REE study of late Triassic dolerites from the Pyrenees
674 (France) and the Messejana Dyke (Spain and Portugal), *Earth and Planetary Science Letters*,
675 73(1), 81-90.

676 Anderson, D. L. (1994), The sublithospheric mantle as the source of continental flood basalts:
677 The case against the continental lithosphere and plume head reservoirs, *Earth and Planetary
678 Science Letters*, 123, 269-280.

679 Armytage, R. M., A. D. Brandon, R. Andreasen, and T. J. Lapen (2015), Evolution of Mojavian
680 mantle lithosphere influenced by Farallon plate subduction: Evidence from Hf and Nd isotopes
681 in peridotite xenoliths from Dish Hill, CA, *Geochimica et Cosmochimica Acta*, 159, 264-284.

682 Baksi, A. K. (2003), Critical evaluation of $^{40}\text{Ar}/^{39}\text{Ar}$ ages for the Central Atlantic Magmatic
683 Province: timing, duration and possible migration of magmatic centers, *Geophysical Monograph*
684 *Series, 136*, 77-90.

685 Banks, H. O. (1950), The determination of the solubility of hafnium oxide in aqueous solution by
686 the radioactive tracer technique, 4822 pp, School of Mines and Metallurgy of the University of
687 Missouri, Rolla, Missouri.

688 Bédard, J. (1992), Jurassic quartz-normative tholeiite dikes from Anticosti Island, Quebec, In
689 *Eastern North American Mesozoic Magmatism*, Eds. Puffer, J.H. and P.C. Ragland, *Special*
690 *Papers-Geological Society of America*, v. 268, 161.

691 Begemann, F., K. Ludwig, G. Lugmair, K. Min, L. Nyquist, P. Patchett, P. Renne, C.-Y. Shih, I.
692 M. Villa, and R. Walker (2001), Call for an improved set of decay constants for
693 geochronological use, *Geochimica et Cosmochimica Acta*, 65(1), 111-121.

694 Béguelin, P., M. Bizimis, C. Beier, and S. Turner (2017), Rift–plume interaction reveals multiple
695 generations of recycled oceanic crust in Azores lavas, *Geochimica et Cosmochimica Acta*, 218,
696 132-152.

697 Bertrand, H. (1991), *The Mesozoic tholeiitic province of Northwest Africa; a volcanotectonic*
698 *record of the early opening of Central Atlantic*, In *Magmatism in extensional structural settings:*
699 *the Phanerozoic African Plate*, Eds. Kampunzu, A.B. and R.T. Lubala, Springer-Verlag, Berlin,
700 Germany.

701 Bertrand, H., J. Dostal, and C. Dupuy (1982), Geochemistry of early Mesozoic tholeiites from
702 Morocco, *Earth and Planetary Science Letters*, 58(2), 225-239.

703 Bindeman, I. N., and O. E. Melnik (2016), Zircon survival, rebirth and recycling during crustal
704 melting, magma crystallization, and mixing based on numerical modelling, *Journal of Petrology*,
705 57(3), 437-460.

706 Blackburn, T. J., P. E. Olsen, S. A. Bowring, N. M. McLean, D. V. Kent, J. Puffer, G. McHone,
707 E. T. Rasbury, and M. Et-Touhami (2013), Zircon U-Pb geochronology links the end-Triassic
708 extinction with the Central Atlantic Magmatic Province, *Science*, 340(6135), 941-945.

709 Blichert-Toft, J. (2001), On the Lu-Hf isotope geochemistry of silicate rocks, *Geostandards*
710 *Newsletter-the Journal of Geostandards and Geoanalysis*, 25(1), 41-56.

711 Blichert-Toft, J., F. A. Frey, and F. Albarede (1999), Hf isotope evidence for pelagic sediments
712 in the source of Hawaiian basalts, *Science*, 285(5429), 879-882.

713 Blichert-Toft, J., A. Agranier, M. Andres, R. Kingsley, J. G. Schilling, and F. Albarede (2005),
714 Geochemical segmentation of the Mid-Atlantic Ridge north of Iceland and ridge-hot spot
715 interaction in the North Atlantic, *Geochemistry Geophysics Geosystems*, 6,
716 10.1029/2004GC000788.

717 Bohron, W. A., and F. J. Spera (2001), Energy-constrained open-system magmatic processes II:
718 application of energy-constrained assimilation–fractional crystallization (EC-AFC) model to
719 magmatic systems, *Journal of Petrology*, 42(5), 1019-1041.

720 Bouvier, A., J. D. Vervoort, and P. J. Patchett (2008), The Lu–Hf and Sm–Nd isotopic
721 composition of CHUR: constraints from unequilibrated chondrites and implications for the bulk
722 composition of terrestrial planets, *Earth and Planetary Science Letters*, 273(1-2), 48-57.

723 Bryan, S. E., and R. E. Ernst (2008), Revised definition of large igneous provinces (LIPs), *Earth-*
724 *Science Reviews*, 86(1-4), 175-202.

725 Burov, E., and T. Gerya (2014), Asymmetric three-dimensional topography over mantle plumes,
726 *Nature*, 513(7516), 85.

727 Callegaro, S., A. Marzoli, H. Bertrand, M. Chiaradia, L. Reisberg, C. Meyzen, G. Bellieni, R. E.
728 Weems, and R. Merle (2013), Upper and lower crust recycling in the source of CAMP basaltic
729 dykes from southeastern North America, *Earth and Planetary Science Letters*, 376, 186-199.

730 Callegaro, S., D.R. Baker, A. De Min, A. Marzoli, K. Geraki, H. Bertrand, C. Viti, and F.
731 Nestola (2014), Enriched mantle source for the Central Atlantic magmatic province: New
732 supporting evidence from southwestern Europe, *Lithos*, 188, 15-32.

733 Callegaro, S., A. Marzoli, H. Bertrand, J. Blichert-Toft, L. Reisberg, G. Cavazzini, F. Jourdan,
734 J.H. Davies, L. Parisio, R. Bouchet, A. Paul, U. Schaltegger, M. Chiaradia (2017), Geochemical
735 Constraints Provided by the Freetown Layered Complex (Sierra Leone) on the Origin of High-Ti
736 Tholeiitic CAMP Magmas, *Journal of Petrology*, 58(9), 1811-1840.

737 Carlson, R. (1991), Physical and chemical evidence on the cause and source characteristics of
738 flood basalt volcanism, *Australian Journal of Earth Sciences*, 38(5), 525-544.

739 Cebriá, J. M., J. López-Ruiz, M. Doblas, L. T. Martins, and J. Munha (2003), Geochemistry of
740 the Early Jurassic Messejana-Plasencia dyke (Portugal-Spain); Implications on the Origin of the
741 Central Atlantic Magmatic Province, *Journal of Petrology*, 44, 547-568.

742 Chabou, M. C., H. Bertrand, and A. Sebaï (2010), Geochemistry of the Central Atlantic
743 Magmatic Province (CAMP) in south-western Algeria, *Journal of African Earth Sciences*, 58,
744 211-219.

745 Chauvel, C., E. Lewin, M. Carpentier, N. T. Arndt, and J. C. Marini (2008), Role of recycled
746 oceanic basalt and sediment in generating the Hf-Nd mantle array, *Nature Geoscience*, 1(1), 64-
747 67.

748 Chauvel, C., E. Lewin, M. Carpentier, N. T. Arndt, and J.-C. Marini (2008), Role of recycled
749 oceanic basalt and sediment in generating the Hf–Nd mantle array, *Nature geoscience*, 1(1), 64.

750 Chauvel, C., M. Garcon, S. Bureau, A. Besnault, B. M. Jahn, and Z. L. Ding (2014), Constraints
751 from loess on the Hf-Nd isotopic composition of the upper continental crust, *Earth and*
752 *Planetary Science Letters*, 388, 48-58.

753 Chen, T.-Y., G. Li, M. Frank, H.-F. Ling (2013), Hafnium isotope fractionation during
754 continental weathering: Implications for the generation of the seawater Nd-Hf isotope
755 relationships, *Geophysical Research Letters*, 40, 916-920.

756 Choi, S. H., S. B. Mukasa, X.-H. Zhou, X. H. Xian, and A. V. Andronikov (2008), Mantle
757 dynamics beneath East Asia constrained by Sr, Nd, Pb and Hf isotopic systematics of ultramafic
758 xenoliths and their host basalts from Hannuoba, North China, *Chemical Geology*, 248(1-2), 40-
759 61.

760 Choi, S. H., K. Suzuki, S. B. Mukasa, J. I. Lee, and H. Jung (2010), Lu-Hf and Re-Os
761 systematics of peridotite xenoliths from Spitsbergen, western Svalbard: Implications for mantle-
762 crust coupling, *Earth and Planetary Science Letters*, 297(1-2), 121-132.

763 Cirilli, S., A. Marzoli, L. Tanner, H. Bertrand, N. Buratti, F. Jourdan, G. Bellieni, D. Kontak, and
764 P. R. Renne (2009), Latest Triassic onset of the Central Atlantic Magmatic Province (CAMP)
765 volcanism in the Fundy Basin (Nova Scotia): New stratigraphic constraints, *Earth and Planetary*
766 *Science Letters*, 286, 514-525.

767 Coffin, M. F., and O. Eldholm (1992), Volcanism and continental break-up; a global compilation
768 of large igneous provinces, *Geological Society Special Publications*, 68, 17-30.

769 Coltice, N., B. Phillips, H. Bertrand, Y. Ricard, and P. Rey (2007), Global warming of the
770 mantle at the origin of flood basalts over supercontinents, *Geology*, 35(5), 391-394.

771 Courtillot, V., C. Jaupart, I. Manighetti, P. Tapponnier, and J. Besse (1999), On causal links
772 between flood basalts and continental breakup, *Earth and Planetary Science Letters*, 166, 177-
773 195.

774 Davies, J. H. F. L., A. Marzoli, H. Bertrand, N. Youbi, M. Ernesto, and U. Schaltegger (2017),
775 End-Triassic mass extinction started by intrusive CAMP activity, *Nature Communications*, 8,
776 15596.

777 De Boer, J. (1992), Stress configurations during and following emplacement of ENA basalts in
778 the northern Appalachians, In *Eastern North American Mesozoic Magmatism*, Eds. Puffer, J.H.
779 and P.C. Ragland, *Special Papers-Geological Society of America*, 268, 361.

780 De Min, A., E. M. Piccirillo, A. Marzoli, G. Bellieni, P. R. Renne, M. Ernesto, and L. S.
781 Marques (2003), The Central Atlantic Magmatic Province (CAMP) in Brazil: petrology,
782 geochemistry, $^{40}\text{Ar}/^{39}\text{Ar}$ ages, paleomagnetism and geodynamic implications, *Geophysical*
783 *Monograph Series*, 136, 91-128.

784 Deckart, K., G. Féraud, and H. Bertrand (1997), Age of Jurassic continental tholeiites of French
785 Guyana, Surinam and Guinea: Implications for the initial opening of the Central Atlantic Ocean,
786 *Earth and Planetary Science Letters*, 150, 205-220.

787 Deckart, K., H. Bertrand, and J.-P. Liégeois (2005), Geochemistry and Sr, Nd, Pb isotopic
788 composition of the Central Atlantic Magmatic Province (CAMP) in Guyana and Guinea, *Lithos*,
789 82, 289-314.

790 Dorais, M. J., and M. Tubrett (2008), Identification of a subduction zone component in the
791 Higganum dike, Central Atlantic Magmatic Province: A LA-ICPMS study of clinopyroxene with
792 implications for flood basalt petrogenesis, *Geochemistry, Geophysics, Geosystems*, 9(10).

793 Dorais, M. J., M. Harper, S. Larson, H. Nugroho, P. Richardson, and N. Roosmawati (2005), A
794 comparison of Eastern North America and Coastal New England magma suites: implications for
795 subcontinental mantle evolution and the broad-terrane hypothesis, *Canadian Journal Earth Sci*,
796 42(1571-1587).

797 Dostal, J., and C. Dupuy (1984), Geochemistry of the North Mountain Basalts (Nova Scotia,
798 Canada), *Chemical Geology*, 45(3), 245-261.

799 Dostal, J., and M. Durning (1998), Geochemical constraints on the origin and evolution of early
800 Mesozoic dikes in Atlantic Canada, *European Journal Mineralogy*, 10, 79-93.

801 Dunning, G. R., and J. P. Hodych (1990), U/Pb zircon and baddeleyite ages for the Palisades and
802 Gettysburg sills of the northeastern United States: Implications for the age of the
803 Triassic/Jurassic boundary, *Geology*, 18, 795-798.

804 Dupuy, C., J. Marsh, J. Dostal, A. Michard, and S. Testa (1988), Asthenospheric and lithospheric
805 sources for Mesozoic dolerites from Liberia (Africa): trace element and isotopic evidence, *Earth
806 and Planetary Science Letters*, 87(1), 100-110.

807 Eisele, J., M. Sharma, S. J. Galer, J. Blichert-Toft, C. W. Devey, and A. W. Hofmann (2002),
808 The role of sediment recycling in EM-1 inferred from Os, Pb, Hf, Nd, Sr isotope and trace
809 element systematics of the Pitcairn hotspot, *Earth and Planetary Science Letters*, 196(3), 197-
810 212.

811 Ernst, R. E., and K. L. Buchan (2003), Recognizing Mantle Plumes in the Geological Record,
812 *Annual Reviews Earth Planetary Science*, 31, 469-523.

813 Ernst, R. E., E. B. Grosfils, and D. Mège (2001), Giant Dike Swarms: Earth, Venus, and Mars,
814 *Annual Reviews Earth Planetary Science*, 29, 489-534.

815 Falloon, T.J. and L.V. Danyushevsky (2000), Melting of refractory mantle at 1.5, 2 and 2.5 GPa
816 under anhydrous and H₂O-undersaturated conditions: Implications for the petrogenesis of high-
817 Ca boninites and the influence of subduction components on mantle melting, *Journal of
818 Petrology*, 41(2), 257-283.

819 Frisby, C., M. Bizimis, and S. Mallick (2016), Hf-Nd isotope decoupling in bulk abyssal
820 peridotites due to serpentinization, *Chemical Geology*, 440, 60-72.

821 Garcon, M., C. Chauvel, C. France-Lanord, P. Huyghe, and J. Lave (2013), Continental
822 sedimentary processes decouple Nd and Hf isotopes, *Geochimica Et Cosmochimica Acta*, 121,
823 177-195.

824 Garcon, M., C. Chauvel, C. France-Lanord, M. Limonta, and E. Garzanti (2014), Which minerals
825 control the Nd-Hf-Sr-Pb isotopic compositions of river sediments?, *Chemical Geology*, 364, 42-
826 55.

827 Geldmacher, J., K. Hoernle, B. B. Hanan, J. Blichert-Toft, F. Hauff, J. B. Gill, and H.-U.
828 Schmincke (2011), Hafnium isotopic variations in East Atlantic intraplate volcanism,
829 *Contributions to Mineralogy and Petrology*, 162(1), 21-36.

830 Gillard, M., D. Sauter, J. Tugend, S. Tomasi, M.-E. Epin, and G. Manatschal (2017), Birth of an
831 oceanic spreading center at a magma-poor rift system, *Scientific reports*, 7(1), 15072.

832 Griffin, W., N. Pearson, E. Belousova, S. v. Jackson, E. Van Achtebergh, S. Y. O'Reilly, and S.
833 Shee (2000), The Hf isotope composition of cratonic mantle: LAM-MC-ICPMS analysis of
834 zircon megacrysts in kimberlites, *Geochimica et Cosmochimica Acta*, 64(1), 133-147.

835 Guo, W., S. Zhao, F. Wang, Z. Yang, S. Jia, and Z. Liu (2019), Crustal structure of the eastern
836 Piedmont and Atlantic coastal plain in North Carolina and Virginia, eastern North American
837 margin, *Earth, Planets and Space*, 71(1), 69.

838 Halliday, A. N., A. P. Dickin, R. N. Hunter, G. R. Davies, T. J. Dempster, P. J. Hamilton, and B.
839 G. Upton (1993), Formation and composition of the lower continental crust: evidence from
840 Scottish xenolith suites, *Journal of Geophysical Research: Solid Earth*, 98(B1), 581-607.

841 Hames, W. E., P. R. Renne, and C. Ruppel (2000), New evidence for geologically instantaneous
842 emplacement of earliest Jurassic Central Atlantic magmatic province basalts on the North
843 American margin, *Geology*, 28, 859-862.

844 Heatherington, A. L., and P. A. Mueller (1999), Lithospheric sources of North Florida, USA
845 tholeiites and implications for the origin of the Suwannee terrane, *Lithos*, 46, 215-233.

846 Heimdal, T. H., H. H. Svensen, J. Ramezani, K. Iyer, E. Pereira, R. Rodrigues, M. T. Jones, and
847 S. Callegaro (2018), Large-scale sill emplacement in Brazil as a trigger for the end-Triassic
848 crisis, *Scientific Reports*, 8, 141.

849 Hermes, O. (1964), A quantitative petrographic study of dolerite in the Deep River Basin, North
850 Carolina, *Am. Mineral*, 49, 1718-1729.

851 Herzberg, C., and E. Gazel (2009), Petrological evidence for secular cooling in mantle plumes,
852 *Nature*, 458(7238), 619.

853 Hesselbo, S. P., S. A. Robinson, F. Surlyk, and S. Piasecki (2002), Terrestrial and marine
854 extinction at the Triassic-Jurassic boundary synchronized with major carbon-cycle perturbation:
855 A link to initiation of massive volcanism?, *Geology*, 30(3), 251-254.

856 Hill, R. I. (1991), Starting plumes and continental break-up, *Earth and Planetary Science*
857 *Letters*, 104(2), 398-416.

858 Hodych, J. P., and G. R. Dunning (1992), Did the Manicouagan impact trigger end-of-Triassic
859 mass extinction?, *Geology*, 20, 51-54.

860 Holbrook, W., and P. Kelemen (1993), Large igneous province on the US Atlantic margin and
861 implications for magmatism during continental breakup, *Nature*, 364(6436), 433-436.

862 Holbrook, W. S., E. Reiter, G. Purdy, D. Sawyer, P. Stoffa, J. Austin Jr, J. Oh, and J. Makris
863 (1994), Deep structure of the US Atlantic continental margin, offshore South Carolina, from

864 coincident ocean bottom and multichannel seismic data, *Journal of Geophysical Research*,
865 99(B5), 9155-9178.

866 Hole, M. J. (2015), The generation of continental flood basalts by decompression melting of
867 internally heated mantle, *Geology*, 43(4), 311-314.

868 Huang, Y.-M., P. Van Calsteren, and C. I. Hawkesworth (1995), The evolution of the lithosphere
869 in southern Africa: a perspective on the basic granulite xenoliths from kimberlites in South
870 Africa, *Geochimica et Cosmochimica Acta*, 59(23), 4905-4920.

871 Iacumin, M., A. De Min, E. M. Piccirillo, and G. Bellieni (2003), Source mantle heterogeneity
872 and its role in the genesis of Late Archaean-Proterozoic (2.7-1.0 Ga) and Mesozoic (200 and 130
873 Ma) tholeiitic magmatism in the South American Platform, *Earth-Science Reviews*, 62, 365-397.

874 Ingle, S., P. A. Mueller, A. L. Heatherington, and M. Kozuch (2003), Isotopic evidence for the
875 magmatic and tectonic histories of the Carolina terrane: implications for stratigraphy and terrane
876 affiliation, *Tectonophysics*, 371(1-4), 187-211.

877 Jackson, M.G., S.R. Hart, A.P. Koppers, H. Staudigel, J. Konter, J. Blusztajn, M. Kurz, and J.A.
878 Russell (2007), The return of subducted continental crust in Samoan lavas, *Nature*, 448, 684-687.

879 Jackson, M. G., and R. Dasgupta (2008), Compositions of HIMU, EM1, and EM2 from global
880 trends between radiogenic isotopes and major elements in ocean island basalts, *Earth and
881 Planetary Science Letters*, 276(1-2), 175-186.

882 Jaffey, A. H., K. F. Flynn, Glendeni.Le, W. C. Bentley, and A. M. Essling (1971), Precision
883 Measurement of Half-Lives and Specific Activities of U-235 and U-238, *Physical Review C*,
884 4(5), 1889-1906.

885 Janney, P. E., and P. R. Castillo (2001), Geochemistry of the oldest Atlantic oceanic crust
886 suggests mantle plume involvement in the early history of the central Atlantic Ocean, *Earth and*
887 *Planetary Science Letters*, 192, 291-302.

888 Janney, P., A. Le Roex, and R. Carlson (2005), Hafnium isotope and trace element constraints on
889 the nature of mantle heterogeneity beneath the central Southwest Indian Ridge (13 E to 47 E),
890 *Journal of Petrology*, 46(12), 2427-2464.

891 Johnson, M. C., and T. Plank (2000), Dehydration and melting experiments constrain the fate of
892 subducted sediments, *Geochemistry, Geophysics, Geosystems*, 1(12), doi:
893 10.1029/1999GC000014.

894 Jourdan, F., A. Marzoli, H. Bertrand, M. Cosca, and D. Fontignie (2003), The northernmost
895 CAMP: $^{40}\text{Ar}/^{39}\text{Ar}$ age, petrology and Sr-Nd-Pb isotope geochemistry of the Kerforne dike,
896 Brittany, France, *Geophysical Monograph Series*, 136, 209-226.

897 Jourdan, F., H. Bertrand, U. Schärer, J. Blichert-Toft, G. Féraud, and A. B. Kampunzu (2007),
898 Major and trace element and Sr, Nd, Hf, and Pb isotope compositions of the Karoo Large
899 Igneous Province, Botswana-Zimbabwe: Lithosphere vs mantle plume contribution, *Journal of*
900 *Petrology*, 48(6), 1043-1077.

901 Jourdan, F., A. Marzoli, H. Bertrand, S. Cirilli, L. H. Tanner, D. J. Kontak, G. McHone, P. R.
902 Renne, and G. Bellieni (2009), $^{40}\text{Ar}/^{39}\text{Ar}$ ages of CAMP in North America: Implications for the
903 Triassic-Jurassic boundary and the ^{40}K decay constant bias, *Lithos*, *110*, 167-180.

904 Kempton, P. D., H. Downes, and M. Lustrino (2018), Pb and Hf isotope evidence for mantle
905 enrichment processes and melt interactions in the lower crust and lithospheric mantle in Miocene
906 orogenic volcanic rocks from Monte Arcuentu (Sardinia, Italy), *Geosphere*, *14*(3), 926-950.

907 Kent, R. (1991), Lithospheric uplift in eastern Gondwana: Evidence for a long-lived mantle
908 plume system?, *Geology*, *19*(1), 19-23.

909 Khanna, T., M. Bizimis, G. Yogodzinski, and S. Mallick (2014), Hafnium-neodymium isotope
910 systematics of the 2.7 Ga Gadwal greenstone terrane, Eastern Dharwar craton, India:
911 Implications for the evolution of the Archean depleted mantle, *Geochimica Et Cosmochimica*
912 *Acta*, *127*, 10-24.

913 Klein, E. M. (2004), Geochemistry of the Igneous Ocean Crust, in *Treatise on Geochemistry*,
914 edited by H. D. Holland and K. K. Turekian, pp. 433-463, Elsevier, Amsterdam.

915 Knight, K. B., S. Nomade, P. R. Renne, A. Marzoli, H. Bertrand, and N. Youbi (2004), The
916 Central Atlantic Magmatic Province at the Triassic-Jurassic boundary: paleomagnetic and
917 $^{40}\text{Ar}/^{39}\text{Ar}$ evidence from Morocco for brief, episodic volcanism, *Earth and Planetary Science*
918 *Letters*, *228*, 143-160.

919 Kogiso, T., Y. Tatsumi, and S. Nakano (1997), Trace element transport during dehydration
920 processes in the subducted oceanic crust: 1. Experiments and implications for the origin of ocean
921 island basalts, *Earth and Planetary Science Letters*, *148*(1-2), 193-205.

922 Kontak, D. J. (2008), On the edge of CAMP: Geology and volcanology of the Jurassic North
923 Mountain Basalt, Nova Scotia, *Lithos*, 101, 74-101.

924 Koptev, A., E. Calais, E. Burov, S. Leroy, and T. Gerya (2015), Dual continental rift systems
925 generated by plume–lithosphere interaction, *Nature Geoscience*, 8(5), 388.

926 Linnen, R. L. (1998), The solubility of Nb-Ta-Zr-Hf-W in granitic melts with Li and Li + F;
927 constraints for mineralization in rare metal granites and pegmatites, *Economic Geology*, 93,
928 1013-1025.

929 Lizarralde, D., and W. S. Holbrook (1997), US mid-Atlantic margin structure and early thermal
930 evolution, *Journal of Geophysical Research*, 102, 22.

931 Magni, V. and A. Király (2019), Delamination, Reference Module in Earth Systems and
932 Environmental Sciences, Elsevier.

933 Mallick, S., J. J. Standish, and M. Bizimis (2015), Constraints on the mantle mineralogy of an
934 ultra-slow ridge: Hafnium isotopes in abyssal peridotites and basalts from the 9-25°E Southwest
935 Indian Ridge, *Earth and Planetary Science Letters*, 410, 42-53.

936 Marsh, J. S. (1987), Basalt geochemistry and tectonic discrimination within continental flood
937 basalt provinces, *Journal of Volcanology and Geothermal Research*, 32(1-3), 35-49.

938 Marzoli, A., P. R. Renne, E. M. Piccirillo, M. Ernesto, G. Bellieni, and A. De Min (1999),
939 Extensive 200-Million-Year-Old Continental Flood Basalts of the Central Atlantic Magmatic
940 Province, *Science*, 284, 616-618.

941 Marzoli, A., H. Bertrand, K.B. Knight, S. Cirilli, C. Verati, S. Nomade, P.R. Renne, N. Youbi, R.
942 Martini, K. Allenbach, R. Neuwerth, C. Rapaille, L. Zaninetti, and G. Bellieni (2004), Synchrony
943 of the Central Atlantic magmatic province and the Triassis-Jurassic boundary climatic and biotic
944 crisis, *Geology*, 32, 973-976.

945 Marzoli, A., F. Jourdan, J. H. Puffer, T. Cuppone, L. H. Tanner, R. E. Weems, H. Bertrand, S.
946 Cirilli, G. Bellieni, and A. De Min (2011), Timing and duration of the Central Atlantic magmatic
947 province in the Newark and Culpeper basins, eastern U.S.A., *Lithos*, 122, 175-188.

948 Marzoli, A., F. Jourdan, F. Bussy, M. Chiaradia, and F. Costa (2014), Petrogenesis of tholeiitic
949 basalts from the Central Atlantic magmatic province as revealed by mineral major and trace
950 elements and Sr isotopes, *Lithos*, 188, 44-59.

951 Marzoli, A., S. Callegaro, J. Dal Corso, J. H. F. L. Davies, M. Chiaradia, N. Youbi, H. Bertrand,
952 L. Reisberg, R. Merle, and F. Jourdan (2018), The Central Atlantic Magmatic Province (CAMP):
953 A Review, in *The Late Triassic World: Earth in a Time of Transition*, edited by L. H. Tanner, pp.
954 91-125, Springer International Publishing, Cham.

955 Marzoli, A., H. Bertrand, N. Youbi, S. Callegaro, R. Merle, L. Reisberg, M. Chiaradia, S.
956 Brownlee, F. Jourdan, and A. Zanetti (2019), The Central Atlantic magmatic province (CAMP)
957 in Morocco, *Journal of Petrology*, 60, 945-996.

958 Mauche, R., G. Faure, L. M. Jones, and J. Hoefs (1989), Anomalous isotopic compositions of Sr,
959 Ar and O in the Mesozoic diabase dikes of Liberia, West Africa, *Contributions to Mineralogy
960 and Petrology*, 101(1), 12-18.

961 May, P. R. (1971), Pattern of Triassic-Jurassic Diabase Dikes around the North Atlantic in the
962 Context of Predrift Position of the Continents, *Geological Society of America Bulletin*, 82, 1285-
963 1292.

964 Mazza, S. E., E. Gazel, E. A. Johnson, M. Bizimis, R. McAleer, and C. B. Biryol (2017),
965 Post-rift magmatic evolution of the eastern North American “passive-aggressive” margin,
966 *Geochemistry, Geophysics, Geosystems*, 18(1), 3-22.

967 Mazza, S. E., E. Gazel, M. Bizimis, R. Moucha, P. Béguelin, E. A. Johnson, R. J. McAleer, and
968 A. V. Sobolev (2019), Sampling the volatile-rich transition zone beneath Bermuda, *Nature*,
969 569(7756), 398.

970 McHone, J. G. (1978), Distribution, orientations, and ages of mafic dikes in central New
971 England, *Geological Society of America Bulletin*, 89(11), 1645-1655.

972 McHone, G. (1996), Broad-terrane Jurassic flood basalts across northeastern North America,
973 *Geology*, 24, 319-322.

974 McHone, J. G. (2000), Non-plume magmatism and rifting during the opening of the central
975 Atlantic Ocean, *Tectonophysics*, 316, 287-296.

976 McKenzie, D., and R. O’Nions (1991), Partial Melt Distributions From Inversion Of Rare-Earth
977 Element Concentrations, *Journal of Petrology*, 32, 1021.

978 Merle, R., A. Marzoli, H. Bertrand, L. Reisberg, C. Verati, C. Zimmermann, M. Chiaradia, and
979 G. Bellieni (2011), $^{40}\text{Ar}/^{39}\text{Ar}$ ages and Sr-Nd-Pb-Os geochemistry of CAMP tholeiites from
980 Western Maranhao basin (NE Brazil), *Lithos*, 122, 137-151.

981 Merle, R., A. Marzoli, L. Reisberg, H. Bertrand, A. Nemchin, M. Chiaradia, S. Callegaro, F.
982 Jourdan, G. Bellieni, D. Kontak, J. Puffer, and J.G. McHone (2014), Sr, Nd, Pb and Os Isotope
983 Systematics of CAMP Tholeiites from Eastern North America (ENA): Evidence of a
984 Subduction-enriched Mantle Source, *Journal of Petrology*, 55(1), 133-180.

985 Morgan, P. (1983), Constraints on rift thermal processes from heat flow and uplift,
986 *Tectonophysics*, 94(1), 277-298.

987 Münker, C., S. Weyer, E. Scherer, and K. Mezger (2001), Separation of high field strength
988 elements (Nb, Ta, Zr, Hf) and Lu from rock samples for MC-ICPMS measurements, *Geochem.*
989 *Geophys. Geosyst.*, 2(12), doi: 10.1029/2001GC000183.

990 Nehring, F., S.F. Foley, and P. Hölttä (2010), Trace element partitioning in the granulite facies,
991 *Contrib. Mineral. Petrol.*, 159, 493-519.

992 Nomade, S., K. Knight, E. Beutel, P. Renne, C. Verati, G. Féraud, A. Marzoli, N. Youbi, and H.
993 Bertrand (2007), Chronology of the Central Atlantic Magmatic Province: Implications for the
994 Central Atlantic rifting processes and the Triassic-Jurassic biotic crisis, *Palaeogeography,*
995 *Palaeoclimatology, Palaeoecology*, 244(1), 326-344.

996 Oyarzun, R., M. Doblas, J. López-Ruiz, and J. M. Cebriá (1997), Opening of the central Atlantic
997 and asymmetric mantle upwelling phenomena: implications for long-lived magmatism in western
998 North Africa and Europe, *Geology*, 25(8), 727-730.

999 Papezik, V., J. D. Greenough, J. A. Colwell, and T. J. Mallinson (1988), North Mountain basalt
1000 from Digby, Nova Scotia: models for a fissure eruption from stratigraphy and petrochemistry,
1001 *Canadian Journal of Earth Sciences*, 25(1), 74-83.

1002 Pe-Piper, G., and D. J. W. Piper (1999), Were Jurassic tholeiitic lavas originally widespread in
1003 southeastern Canada?: a test of the broad terrane hypothesis, *Canadian Journal of Earth*
1004 *Sciences*, 36(9), 1509-1516.

1005 Pegram, W. J. (1990), Development of continental lithospheric mantle as reflected in the
1006 chemistry of the Mesozoic Appalachian tholeiites, USA, *Earth and Planetary Science Letters*,
1007 97(3), 316-331.

1008 Pettingill, H. S., A. Sinha, and M. Tatsumoto (1984), Age and origin of anorthosites,
1009 charnockites, and granulites in the central Virginia Blue Ridge: Nd and Sr isotopic evidence,
1010 *Contributions to Mineralogy and Petrology*, 85(3), 279-291.

1011 Plank, T., and C. H. Langmuir (1998), The chemical composition of subducting sediment and its
1012 consequences for the crust and mantle, *Chemical geology*, 145(3), 325-394.

1013 Puffer, J. (1992), Eastern North American flood basalts in the context of the incipient breakup of
1014 Pangea, , In *Eastern North American Mesozoic Magmatism*, Eds. Puffer, J.H. and P.C. Ragland,
1015 *Special Papers-Geological Society of America*, v. 268, 95.

1016 Puffer, J. (2001), Contrasting high field strength element contents of continental flood basalts
1017 from plume versus reactivated-arc sources, *Geology*, 29(8), 675-678.

1018 Puffer, J. H. (2003), A reactivated back-arc source for CAMP magma, *Geophysical Monograph*
1019 *Series*, 136, 151-162.

- 1020 Puffer, J., D. Hurtubise, F. Geiger, and P. Lechler (1981), Chemical composition and
1021 stratigraphic correlation of the Mesozoic basalt units of the Newark Basin, New Jersey, and the
1022 Hartford Basin, Connecticut, *Geological Society of America Bulletin*, 92, 515-553.
- 1023 Ragland, P., L. Cummins, and J. Arthur (1992), Compositional patterns for early Mesozoic
1024 diabases from South Carolina to central Virginia, In *Eastern North American Mesozoic*
1025 *Magmatism*, Eds. Puffer, J.H. and P.C. Ragland, *Special Papers-Geological Society of America*,
1026 v. 268, 309.
- 1027 Reinemund, J. A. (1955), *Geology of the Deep River coal field, North Carolina*, Geological
1028 Survey Professional Paper 246, U.S. Government Printing Office, Washington, D.C.
- 1029 Rey, P. F. (2015), The geodynamics of mantle melting, *Geology*, 43(4), 367-368.
- 1030 Ruiz-Martínez, V. C., T. H. Torsvik, D. J. J. van Hinsbergen, and C. Gaina (2012), Earth at
1031 200Ma: Global palaeogeography refined from CAMP palaeomagnetic data, *Earth and Planetary*
1032 *Science Letters*, 331, 67-79.
- 1033 Salters, V. J. M., and S. R. Hart (1989), The Hafnium Paradox and the Role of Garnet in the
1034 Source of Mid-Ocean-Ridge Basalts, *Nature*, 342(6248), 420-422.
- 1035 Salters, V. J., and A. Stracke (2004), Composition of the depleted mantle, *Geochemistry*,
1036 *Geophysics, Geosystems*, 5(5), doi: 10.1029/2003GC000597.
- 1037 Salters, V. J., J. Blichert-Toft, Z. Fekiacova, A. Sachi-Kocher, and M. Bizimis (2006), Isotope
1038 and trace element evidence for depleted lithosphere in the source of enriched Ko'olau basalts,
1039 *Contributions to Mineralogy and Petrology*, 151(3), 297-312.

1040 Salters, V. J., S. Mallick, S. R. Hart, C. E. Langmuir, and A. Stracke (2011), Domains of
1041 depleted mantle: New evidence from hafnium and neodymium isotopes, *Geochemistry,*
1042 *Geophysics, Geosystems, 12*(8), doi: 10.1029/2011GC003617.

1043 Saunders, A. D., S. M. Jones, L. A. Morgan, K. L. Pierce, M. Widdowson, and Y. G. Xu (2007),
1044 Regional uplift associated with continental large igneous provinces; the roles of mantle plumes
1045 and the lithosphere, *Chemical Geology, 241*(3-4), 282-318.

1046 Schmitz, M. D., J. D. Vervoort, S. A. Bowring, and P. J. Patchett (2004), Decoupling of the Lu-
1047 Hf and Sm-Nd isotope systems during the evolution of granulitic lower crust beneath southern
1048 Africa, *Geology, 32*(5), 405-408.

1049 Sebai, A., G. Feraud, H. Bertrand, and J. Hanes (1991), $^{40}\text{Ar}/^{39}\text{Ar}$ dating and geochemistry of
1050 tholeiitic magmatism related to the early opening of the Central Atlantic Rift, *Earth and*
1051 *Planetary Science Letters, 104*(2), 455-472.

1052 Sengör, A., and K. Burke (1978), Relative timing of rifting and volcanism on Earth and its
1053 tectonic implications, *Geophysical Research Letters, 5*(6), 419-421.

1054 Shaw, J., J. Baker, A. Kent, K. Ibrahim, and M. Menzies (2007), The geochemistry of the
1055 Arabian lithospheric mantle—a source for intraplate volcanism?, *Journal of Petrology, 48*(8),
1056 1495-1512.

1057 Shellnutt, J. G., J. Dostal, and M.-W. Yeh (2018), Mantle source heterogeneity of the Early
1058 Jurassic basalt of eastern North America, *International Journal of Earth Sciences, 107*(3), 1033-
1059 1058.

1060 Sinha, A., J. Hogan, and J. Parks (1996), Lead Isotope Mapping of Crustal Reservoirs Within the
1061 Grenville Supertectonic: I. Central and Southern Appalachians, *Geophysical Monograph-*
1062 *American Geophysical Union*, 95, 293-306.

1063 Sobolev, S. V., A. V. Sobolev, D. V. Kuzmin, N. A. Krivolutskaya, A. G. Petrunin, N. T. Arndt,
1064 V. A. Radko, and Y. R. Vasiliev (2011), Linking mantle plumes, large igneous provinces and
1065 environmental catastrophes, *Nature*, 477(7364), 312-316.

1066 Söderlund, U., P. J. Patchett, J. D. Vervoort, and C. E. Isachsen (2004), The ^{176}Lu decay constant
1067 determined by Lu–Hf and U–Pb isotope systematics of Precambrian mafic intrusions, *Earth and*
1068 *Planetary Science Letters*, 219(3-4), 311-324.

1069 Spera, F. J., and W. A. Bohrson (2001), Energy-constrained open-system magmatic processes I:
1070 General model and energy-constrained assimilation and fractional crystallization (EC-AFC)
1071 formulation, *Journal of Petrology*, 42(5), 999-1018.

1072 Staudigel, H., T. Plank, B. White, and H. U. Schmincke (1996), Geochemical fluxes during
1073 seafloor alteration of the basaltic upper oceanic crust: DSDP Sites 417 and 418, *Subduction: top*
1074 *to bottom*, 96, 19-38.

1075 Stracke, A., M. Bizimis, and V. J. M. Salters (2003), Recycling oceanic crust: Quantitative
1076 constraints, *Geochemistry, Geophysics, Geosystems*, 4(3), 8003.

1077 Taylor, S. R., and S. M. McLennan (1995), The geochemical evolution of the continental crust,
1078 *Reviews of Geophysics*, 33(2), 241-265.

1079 Tollo, R., and D. Gottfried (1992), Petrochemistry of Jurassic basalt from eight cores, Newark
1080 basin, New Jersey, In *Eastern North American Mesozoic Magmatism*, Eds. Puffer, J.H. and P.C.
1081 Ragland, *Special Papers-Geological Society of America*, v. 268, 233.

1082 Verati, C., H. Bertrand, and G. Féraud (2005), The farthest record of the Central Atlantic
1083 Magmatic Province into West Africa craton: Precise $^{40}\text{Ar}/^{39}\text{Ar}$ dating and geochemistry of
1084 Taoudenni basin intrusives (northern Mali), *Earth and Planetary Science Letters*, 235(1), 391-
1085 407.

1086 Verati, C., C. Rapaille, G. Féraud, A. Marzoli, H. Bertrand, and N. Youbi (2007), $^{40}\text{Ar}/^{39}\text{Ar}$ ages
1087 and duration of the Central Atlantic Magmatic Province volcanism in Morocco and Portugal and
1088 its relation to the Triassic-Jurassic boundary, *Palaeogeography, Palaeoclimatology,*
1089 *Palaeoecology*, 244(1), 308-325.

1090 Vervoort, J. D., P. J. Patchett, J. Blichert-Toft, and F. Albarede (1999), Relationships between
1091 Lu-Hf and Sm-Nd isotopic systems in the global sedimentary system, *Earth and Planetary*
1092 *Science Letters*, 168(1-2), 79-99.

1093 Vervoort, J. D., P. J. Patchett, F. Albarede, J. Blichert-Toft, R. Rudnick, and H. Downes (2000),
1094 Hf-Nd isotopic evolution of the lower crust, *Earth and Planetary Science Letters*, 181(1-2), 115-
1095 129.

1096 Vervoort, J. D., T. Plank, and J. Prytulak (2011), The Hf-Nd isotopic composition of marine
1097 sediments, *Geochimica Et Cosmochimica Acta*, 75, 5903-5926.

1098 Wedepohl, K. H. (1995), The composition of the continental crust, *Geochimica et cosmochimica*
1099 *Acta*, 59(7), 1217-1232.

1100 Weigand, P. W., and P. C. Ragland (1970), Geochemistry of Mesozoic dolerite dikes from
1101 eastern North America, *Contributions to Mineralogy and Petrology*, 29(3), 195-214.

1102 Whalen, L., E. Gazel, C. Vidito, J. Puffer, M. Bizimis, W. Henika, and M. J. Caddick (2015),
1103 Supercontinental inheritance and its influence on supercontinental breakup: The Central Atlantic
1104 Magmatic Province and the breakup of Pangea, *Geochemistry Geophysics Geosystems*, 16(10),
1105 3532-3554.

1106 White, R. S., and D. P. McKenzie (1989), Volcanism at Rifts, *Scientific American*, 261(1), 62-
1107 71.

1108 Willbold, M., and A. Stracke (2006), Trace element composition of mantle end-members:
1109 Implications for recycling of oceanic and upper and lower continental crust, *Geochem. Geophys.*
1110 *Geosyst.*, 7(4), doi: 10.1029/2005GC001005.

1111 Wilson, J. T. (1966), Did the Atlantic close and then re-open?, *Nature*, 211, 676-681.

1112 Wilson, M. (1997), Thermal evolution of the Central Atlantic passive margins: continental
1113 break-up above a Mesozoic super-plume, *Journal of the Geological Society*, 154(3), 491-495.

1114 Wittig, N., J. A. Baker, and H. Downes (2007), U–Th–Pb and Lu–Hf isotopic constraints on the
1115 evolution of sub-continental lithospheric mantle, French Massif Central, *Geochimica et*
1116 *Cosmochimica Acta*, 71(5), 1290-1311.

1117 Wittig, N., D. G. Pearson, S. Duggen, J. A. Baker, and K. Hoernle (2010), Tracing the
1118 metasomatic and magmatic evolution of continental mantle roots with Sr, Nd, Hf and and Pb

1119 isotopes: A case study of Middle Atlas (Morocco) peridotite xenoliths, *Geochimica Et*
1120 *Cosmochimica Acta*, 74(4), 1417-1435.

1121 Woodhead, J. D., and C. W. Devey (1993), Geochemistry of the Pitcairn seamounts, I: source
1122 character and temporal trends, *Earth and Planetary Science Letters*, 116(1-4), 81-99.

1123 Workman, R. K., and S. R. Hart (2005), Major and trace element composition of the depleted
1124 MORB mantle (DMM), *Earth and Planetary Science Letters*, 231, 53-72.

1125 Workman, R. K., S. R. Hart, M. Jackson, M. Regelous, K. Farley, J. Blusztajn, M. Kurz, and H.
1126 Staudigel (2004), Recycled metasomatized lithosphere as the origin of the Enriched Mantle II
1127 (EM2) end-member: Evidence from the Samoan Volcanic Chain, *Geochemistry, Geophysics,*
1128 *Geosystems*, 5(4), doi: 10.1029/2003GC000623.

1129 Wysoczanski, R., J. Gamble, P. Kyle, and M. Thirlwall (1995), The petrology of lower crustal
1130 xenoliths from the Executive Committee Range, Marie Byrd Land volcanic province, West
1131 Antarctica, *Lithos*, 36(3-4), 185-201.

1132 Zartman, R. E., P. D. Kempton, J. B. Paces, H. Downes, I. S. Williams, G. Dobosi, and K. Futral
1133 (2013), Lower-crustal xenoliths from Jurassic kimberlite diatremes, Upper Michigan (USA):
1134 Evidence for Proterozoic Orogenesis and plume magmatism in the lower crust of the Southern
1135 Superior Province, *Journal of Petrology*, 54, 575-608.

1136 Zhao, S., and W. Guo (2019), Crustal Structure of Eastern North Carolina: Piedmont and Coastal
1137 Plain, *Bulletin of the Seismological Society of America*, 109(6), 2288-2304.

1138

1139 **FIGURE CAPTIONS**

1140 Figure 1. Tectonic reconstruction of the central Atlantic region around the time of CAMP
1141 emplacement, with ENA, Morocco, and Sierra Leone sample locations for this study indicated.
1142 Lines and fields in red and yellow indicate locations of CAMP intrusions and lava flows,
1143 respectively (after Deckart et al., 2005, Marzoli et al., 2018). Indicated groupings within CAMP
1144 refer to magma categories defined by Marzoli et al. (2018).

1145 Figure 2. Age-corrected isotope results for samples analyzed in this study, with comparative
1146 values from the literature, for **a.** $\epsilon_{\text{Hf } 201\text{Ma}}$ vs. $\epsilon_{\text{Nd } 201\text{Ma}}$, **b.** $\epsilon_{\text{Hf } 201\text{Ma}}$ vs. $^{206}\text{Pb}/^{204}\text{Pb}_{201\text{Ma}}$, and **c.**
1147 $^{207}\text{Pb}/^{204}\text{Pb}_{201\text{Ma}}$ vs. $^{206}\text{Pb}/^{204}\text{Pb}_{201\text{Ma}}$. Lead and $\epsilon_{\text{Nd } 201\text{Ma}}$ isotope data for samples in this study are
1148 from Callegaro et al. (2013, 2017) and Merle et al. (2014). Other literature data for CAMP are
1149 from Callegaro et al. (2013, 2014, 2017), Deckart et al. (2005), Jourdan et al. (2003), Marzoli et
1150 al. (2019), Merle et al. (2011, 2014), and Whalen et al. (2015), with regional groups defined after
1151 Whalen et al. (2015). End members are shown as black squares, with values as in Table S1 and
1152 described in the text; “GLOSS” refers to global average subducted sediment after Plank and
1153 Langmuir (1998) and Chauvel et al. (2008), aged 170 Ma to represent Paleozoic subducted
1154 sediments (that is, assuming a subduction recycling age of ~370 Ma sampled by CAMP melting
1155 at ~200 Ma, after Callegaro et al. (2013) and Whalen et al. (2015)), “UCC” refers to the average
1156 composition of upper continental crust from the Carolina terrane, and “Mafic LCC,” and
1157 “Intermediate LCC” refer to Proterozoic mafic and intermediate-SiO₂ lower continental crust
1158 compositions, as described in the text and Table S2. Also shown for reference are the ϵ_{Hf} vs. ϵ_{Nd}
1159 mantle array (Vervoort et al., 2011), the field of MORB (Chauvel et al., 2008), the global
1160 seawater array and the field of ferromanganese nodules (after Albarede et al., 1998), average

1161 marine sediments from Chauvel et al. (2014) and Plank and Langmuir (1998), and the field of
1162 Karoo LIP basalts (Jourdan et al., 2007), which exhibits a shallow sloping trend similar to
1163 Hawaiian basalts and our ENA CAMP array. Data sets and compositions unrelated to CAMP are
1164 plotted for reference and have not been age-corrected, except where indicated in the text or data
1165 tables. End-member, age-corrected isotopic compositions for EM-1, EM-2, and DMM were
1166 calculated using the compositions shown in Table S1.

1167 Figure 3. **a.** $\epsilon_{\text{Hf } 201\text{Ma}}$ vs. $\epsilon_{\text{Nd } 201\text{Ma}}$ and **b.** $\epsilon_{\text{Hf } 201\text{Ma}}$ vs. $^{206}\text{Pb}/^{204}\text{Pb}_{201\text{Ma}}$ diagrams for samples from
1168 this study, showing calculated EC-AFC trajectories after Bohrson and Spera (2001) and Spera
1169 and Bohrson (2001), as described in the text and using values from Table S1. Trajectories are
1170 shown for a parent basalt composition similar to sample CS49, which has the most incompatible
1171 element depleted composition based on radiogenic isotope compositions (yellow star; Table 2),
1172 with hypothesized compositions for several upper and lower continental crust assimilants
1173 described in the text and shown in Table S2. The assimilants shown are 1) averaged Carolina
1174 terrane upper continental crust (“Carolina UCC”); 2) a Proterozoic lower crustal mafic granulite
1175 (“Mafic LCC”); and 3) an intermediate lower continental granulite with a hypothesized
1176 $^{206}\text{Pb}/^{204}\text{Pb}_{201\text{Ma}}$ ratio of 17.3, after the discussion in the text (“Intermediate LCC”). Upper
1177 continental crust was calculated using mean compositions of measured Carolina terrane crustal
1178 rocks from Pettingill et al. (1984) and Sinha et al. (1996) and the data compilation of Whalen et
1179 al. (2015). Carolina terrane crustal data set lacks hafnium isotope measurements, so UCC ϵ_{Hf}
1180 $_{201\text{Ma}}$ values were then calculated assuming a relationship with $\epsilon_{\text{Nd } 201\text{Ma}}$ along the terrestrial array
1181 (Vervoort et al., 1999) (Table S1). The Proterozoic mafic granulite shown has elevated Lu/Hf
1182 ratios, similar to average mafic xenoliths from Michigan (Zartman et al., 2013) and
1183 representative of mafic LCC with decoupled ϵ_{Hf} and ϵ_{Nd} . In panel (b), we additionally test mafic

1184 LCC with an alternative Pb isotope composition more closely resembling comparable mafic
1185 granulite xenoliths from Markt, South Africa (Huang et al., 1995) (“Markt LCC”). Intermediate
1186 granulites may have isotopic signatures that record higher time-integrated incompatible element
1187 concentrations than mafic basement (i.e., less radiogenic $^{143}\text{Nd}/^{144}\text{Nd}$ and $^{176}\text{Hf}/^{177}\text{Hf}$ ratios), so
1188 the intermediate LCC composition has a relatively incompatible element-enriched composition
1189 within the range of xenolith measurements by Schmitz et al. (2004). For our intermediate-SiO₂
1190 granulite composition, we also determined partitioning behavior using mineral modes similar to
1191 the intermediate-SiO₂ xenolith sampled by Zartman et al (2013). Tickmarks indicate the
1192 percentage of crustal assimilant added to the magma, up to a maximum of 10% addition. All
1193 other symbols as in Figure 2.

1194 Figure 4. Ternary mixing diagrams for DMM melts, average Carolina terrane continental crust,
1195 and average subducted pelagic marine sediments (GLOSS), as defined in Table S1 and the text,
1196 for **a.** $\epsilon_{\text{Hf } 201\text{Ma}}$ vs. $\epsilon_{\text{Nd } 201\text{Ma}}$, **b.** $\epsilon_{\text{Hf } 201\text{Ma}}$ vs. $^{206}\text{Pb}/^{204}\text{Pb}_{201\text{Ma}}$, and **c.** $^{207}\text{Pb}/^{204}\text{Pb}_{201\text{Ma}}$ vs.
1197 $^{206}\text{Pb}/^{204}\text{Pb}_{201\text{Ma}}$. Mixing lines are plotted in 10% increments; other symbols and mixing
1198 reservoirs as in Figure 2.

1199 Figure 5. Isotope diagrams showing results of isotopic evolution and partial melting calculations
1200 for modified mantle wedge, for **a.** $\epsilon_{\text{Hf } 201\text{Ma}}$ vs. $\epsilon_{\text{Nd } 201\text{Ma}}$, **b.** $\epsilon_{\text{Hf } 201\text{Ma}}$ vs. $^{206}\text{Pb}/^{204}\text{Pb}_{201\text{Ma}}$, and **c.**
1201 $^{207}\text{Pb}/^{204}\text{Pb}_{201\text{Ma}}$ vs. $^{206}\text{Pb}/^{204}\text{Pb}_{201\text{Ma}}$ and with symbols as in Figure 2. The trajectories shown
1202 indicate calculated mantle compositions for a crustal recycling subduction and metasomatism
1203 age of 370 Ma and subsequent mantle melting at 201 Ma. Blue solid lines indicate mantle
1204 compositions when metasomatized by a mixture of fluid derived from altered oceanic crust
1205 (AOC) and fluid derived from subducted global oceanic sediment; “% Sed Fluid” labels indicate

1206 the percentage of sediment-derived fluid in the metasomatizing fluid mixture. Red solid lines
1207 indicate the same, but for AOC-derived fluid and sediment-derived partial melts (with
1208 corresponding “% Sed Melt” labels). Dashed lines and associated labels indicate the amount of
1209 fluid added to the mantle during metasomatism up to 10% addition, as a mass fraction relative to
1210 the initial mantle material (0.01 to 0.10). We note that all fractions of added fluid from 1-10%
1211 addition are compressed into a single narrow zone in panel **c** and so are not labeled. See Table S4
1212 for additional modeling details.

1213 Figure 6. Diagrams showing mixing trajectories between recycled continental crustal rocks and
1214 partial melts of modified, metasomatized mantle, for **a.** $\epsilon_{\text{Hf } 201\text{Ma}}$ vs. $\epsilon_{\text{Nd } 201\text{Ma}}$, **b.** $\epsilon_{\text{Hf } 201\text{Ma}}$ vs.
1215 $^{206}\text{Pb}/^{204}\text{Pb}_{201\text{Ma}}$, and **c.** $^{207}\text{Pb}/^{204}\text{Pb}_{201\text{Ma}}$ vs. $^{206}\text{Pb}/^{204}\text{Pb}_{201\text{Ma}}$ and with mixing lines in 10%
1216 increments and all other symbols as in Figure 2. The “modified mantle” mixing end member is a
1217 calculated 6% batch melt of mantle metasomatized using the methods described in the text and
1218 shown in Figure 5 and Table S4. The example case shown is for mantle modified by 7% addition
1219 of a fluid derived 25% from AOC and 75% from subducted sediments, with a 370 Ma recycling
1220 age and 201 Ma melting age. The UCC composition shown is local Carolina terrane, and the
1221 LCC composition is the “Markt mafic granulite” composition, both from Table S1.

Table 1. Locations and characteristics of samples analyzed for this study, where available.

Sample name	Location description	Latitude (°N)	Longitude (°W)	Outcrop	Reference
<u>Carolinas and Southern ENA:</u>					
CS9	Georgia	34° 45' 21"	83° 29' 33"	Dike	Callegaro et al., 2013
CS26	South Carolina	34° 12' 27"	81° 03' 13"	Dike	Callegaro et al., 2013
CS23	South Carolina	34° 38' 53"	80° 31' 02"	Dike	Callegaro et al., 2013
CS28	South Carolina	34° 39' 08"	80° 31' 01"	Dike	Callegaro et al., 2013
CS14	South Carolina	34° 39' 27"	82° 01' 56"	Dike	Callegaro et al., 2013
CS41	North Carolina	34° 56' 14"	79° 49' 15"	Dike	Callegaro et al., 2013
CS48	North Carolina	35° 04' 15"	79° 50' 38"	Dike	Callegaro et al., 2013
CS46	North Carolina	35° 06' 48"	79° 48' 15"	Dike	Callegaro et al., 2013
CS55	North Carolina	35° 45' 48"	79° 02' 47"	Dike	Callegaro et al., 2013
CS57	North Carolina	35° 50' 11"	79° 00' 48"	Dike	Callegaro et al., 2013
CS49	North Carolina	36° 06' 47"	78° 46' 02"	Sill	Callegaro et al., 2013
CS73	Virginia	37° 17' 44"	78° 27' 38"	Dike	Callegaro et al., 2013
<u>Newark basin:</u>					
NEW03	Palisades Sill			Sill	Merle et al., 2014
NEW136C	Palisades Sill, olivine cumulate layer			Sill	Merle et al., 2014
NEW133	Orange Mountain flow	40° 18' 53"	75° 50' 53"	Lava Flow	Merle et al., 2014
NEW68	Preakness flow	40° 38' 50"	74° 34' 23"	Lava Flow	Merle et al., 2014
NEW52	Preakness flow	40° 40' 33"	74° 24' 32"	Lava Flow	Merle et al., 2014
NEW74	Hook Mountain flow	40° 49' 03"	74° 19' 45"	Lava Flow	Merle et al., 2014
<u>Morocco:</u>					
AN134	Tiourjidal section, basal flow	31° 07' 40"	7° 20' 46"	Lava Flow	Marzoli et al., 2004
<u>Sierra Leone:</u>					
SL45	High-TiO ₂ sample, Freetown Layered Complex, Sierra Leone				Callegaro et al., 2017

Table 2. Hafnium isotope measurements for samples analyzed in this study.

Sample name	Lu (ppm) *	Hf (ppm) *	$^{176}\text{Hf}/^{177}\text{Hf}$	2S **	$\epsilon_{\text{Hf}}^{\text{a}}$	$^{176}\text{Hf}/^{177}\text{Hf}_{201\text{Ma}}$	$\epsilon_{\text{Hf}, 201\text{Ma}}^{\text{a}}$
<u>Carolinas and Southern ENA:</u>							
CS9	0.51	2.02	0.282879	0.000004	3.34	0.282745	3.02
CS26	0.45	1.61	0.282762	0.000004	-0.81	0.282613	-1.64
CS23	0.40	1.68	0.282908	0.000004	4.33	0.282782	4.33
CS28	0.35	1.17	0.282839	0.000003	1.93	0.282683	0.83
CS14	0.42	1.77	0.282753	0.000004	-1.14	0.282626	-1.16
CS41	0.32	0.94	0.282880	0.000004	3.35	0.282698	1.35
CS48	0.35	1.13	0.282826	0.000003	1.47	0.282664	0.17
CS46	0.43	2.54	0.282835	0.000004	1.76	0.282745	3.03
CS55	0.47	1.74	0.282960	0.000002	6.20	0.282818	5.62
CS57	0.37	1.11	0.282883	0.000004	3.46	0.282706	1.65
CS49	0.34	1.33	0.282962	0.000003	6.26	0.282825	5.86
CS73	0.38	1.54	0.282568	0.000003	-7.67	0.282437	-7.85
<u>Newark basin:</u>							
NEW03	0.29	2.95	0.282727	0.000002	-2.06	0.282674	0.53
NEW136C	0.20	1.54	0.282743	0.000004	-1.47	0.282673	0.50
NEW133	0.23	2.37	0.282754	0.000002	-1.11	0.282702	1.50
NEW68	0.25	2.22	0.282849	0.000002	2.26	0.282789	4.57
NEW52	0.35	2.07	0.282794	0.000004	0.32	0.282704	1.58
NEW74	0.62	3.00	0.282930	0.000002	5.13	0.282821	5.71
<u>Morocco:</u>							
AN134	0.31	3.66	0.282769	0.000002	-0.57	0.282724	2.27
<u>Sierra Leone:</u>							
SL45	0.05	0.16	0.282917	0.000005	4.67	0.282785	4.45

* Lutetium and Hf elemental compositions from Callegaro et al. (2013, 2017), Marzoli et al. (2004), and Merle et al. (2013).

** Uncertainties for $^{176}\text{Hf}/^{177}\text{Hf}$ measurements reported as 2S standard errors.

^a ϵ_{Hf} values for measured results calculated using a CHUR $^{176}\text{Hf}/^{177}\text{Hf}$ ratio of 0.282785. Age-corrected ϵ_{Hf} values for 201 Ma were calculated using an adjusted CHUR $^{176}\text{Hf}/^{177}\text{Hf}$ ratio of 0.282659.

Figure 1.

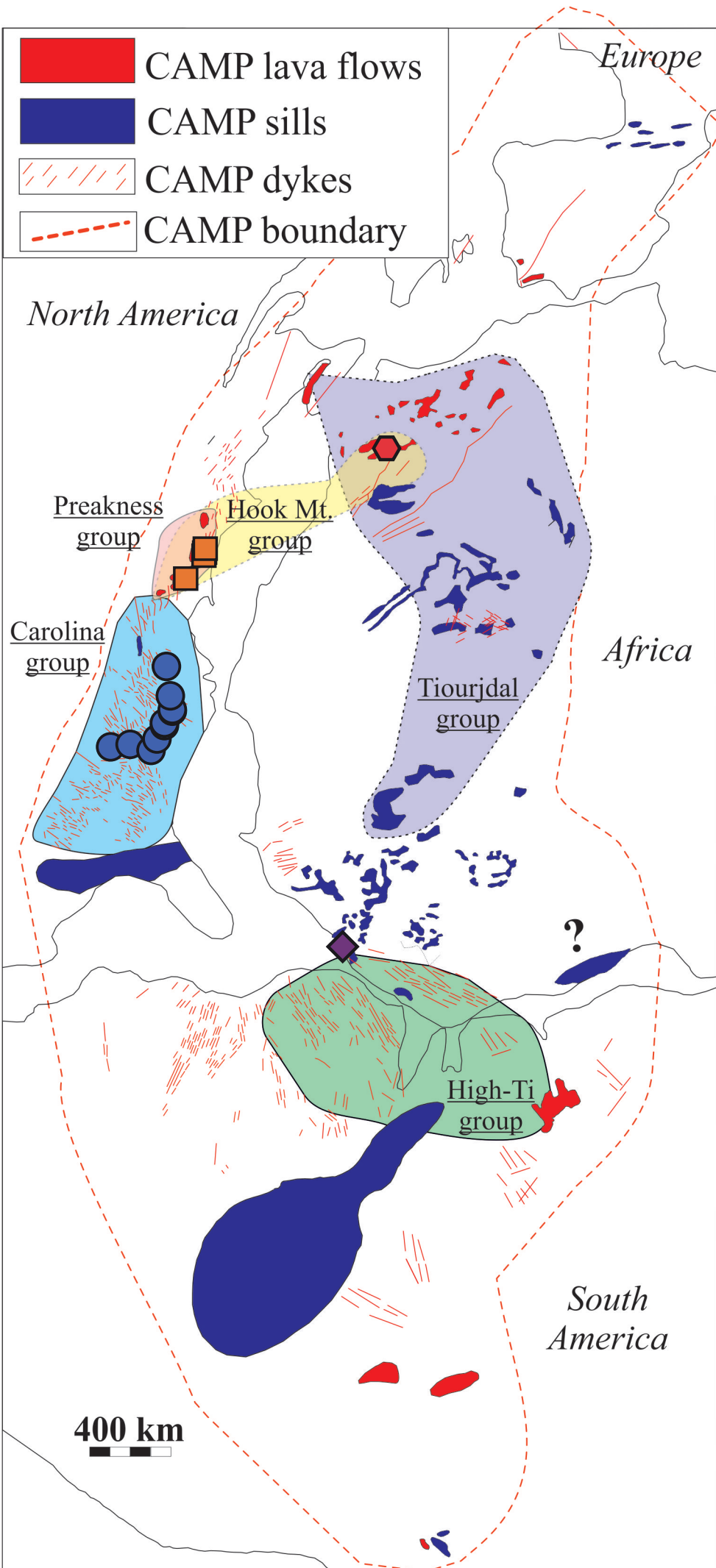
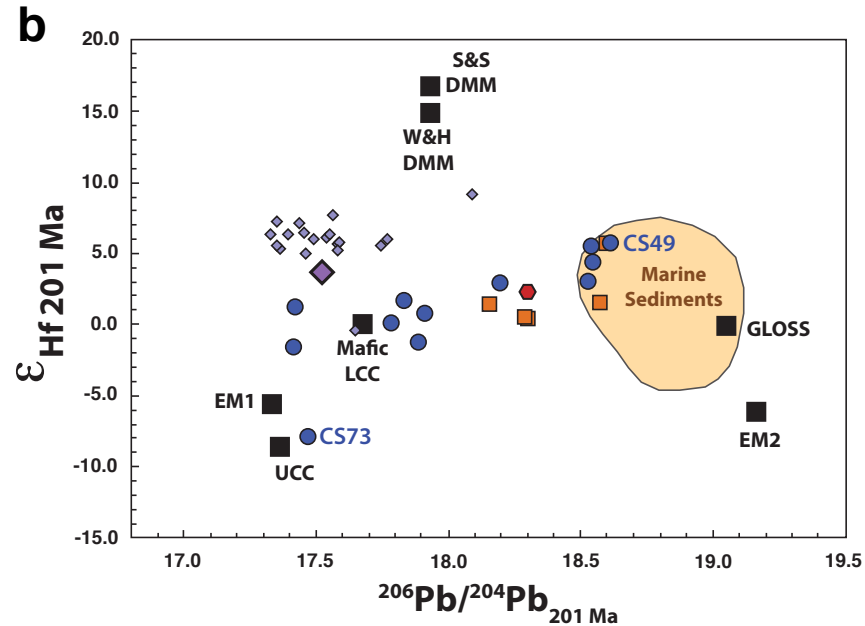
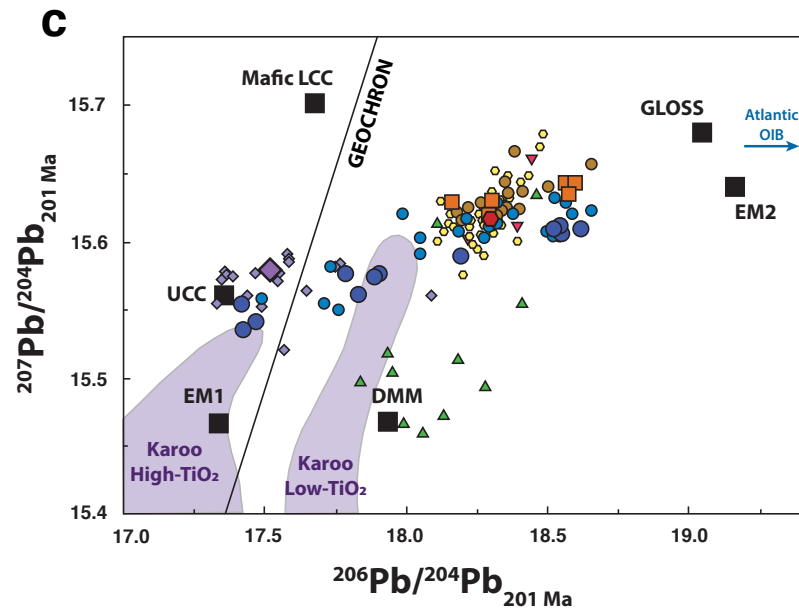
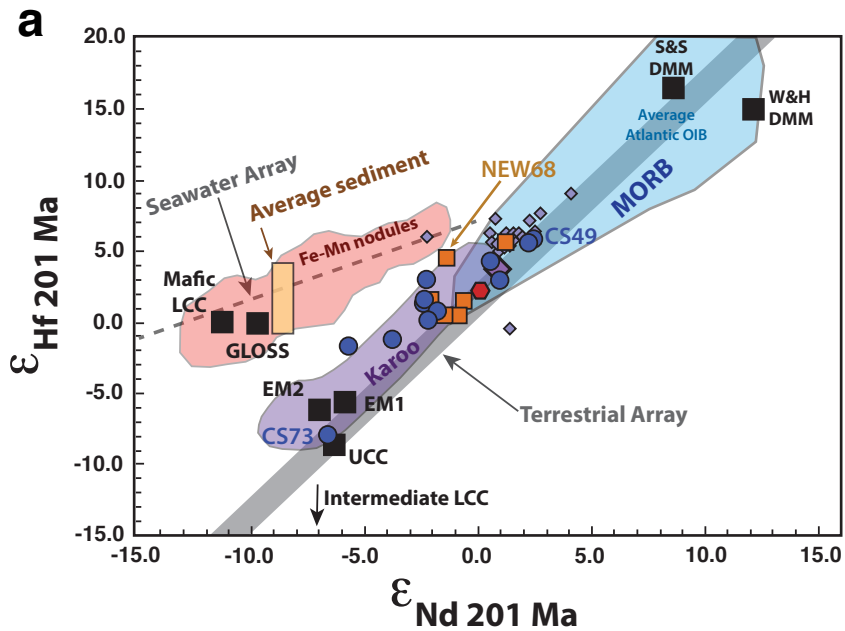


Figure 2.



- Southern ENA (This study)
- Newark Basin (This study)
- Southern ENA
- Northern ENA
- ◆ Sierra Leone (This study)
- ◆ Sierra Leone
- ◆ Morocco (This study)
- European CAMP
- ▼ African CAMP
- ▲ South American CAMP

Figure 3.

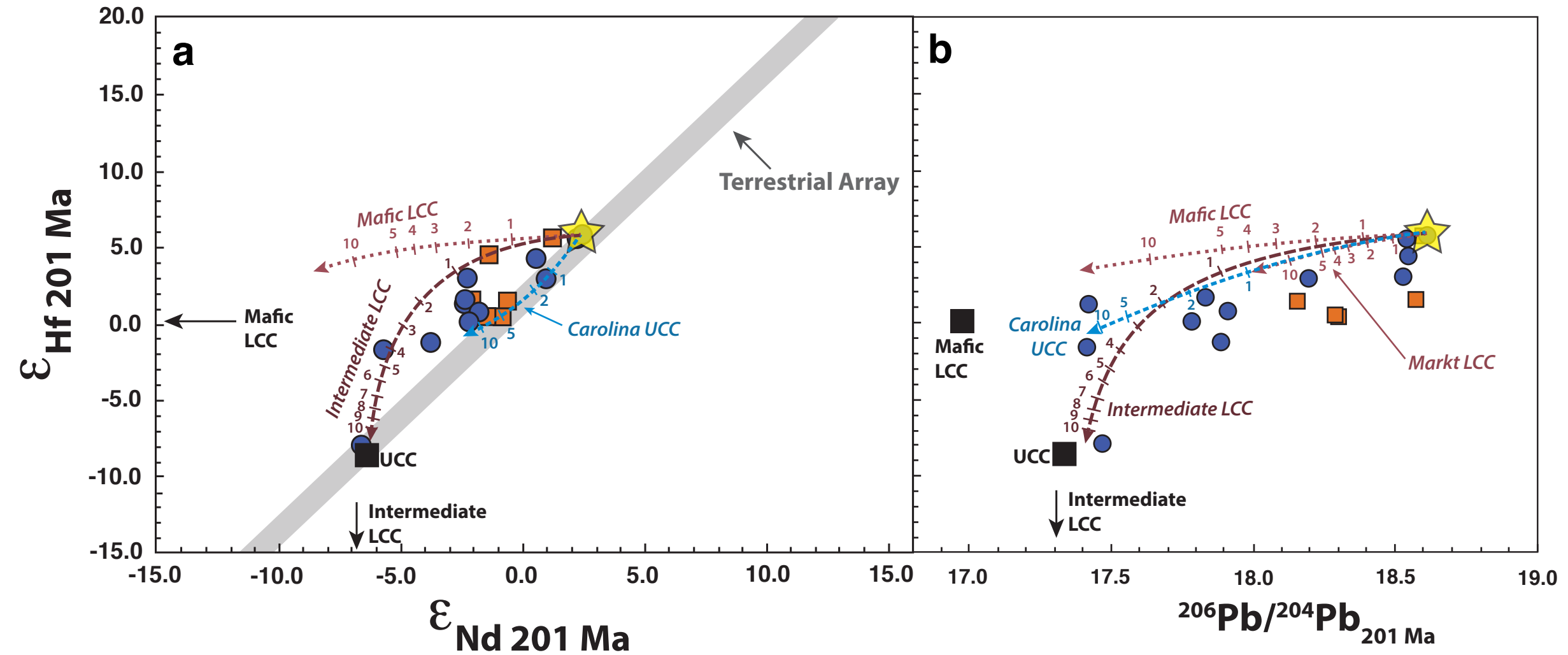


Figure 4.

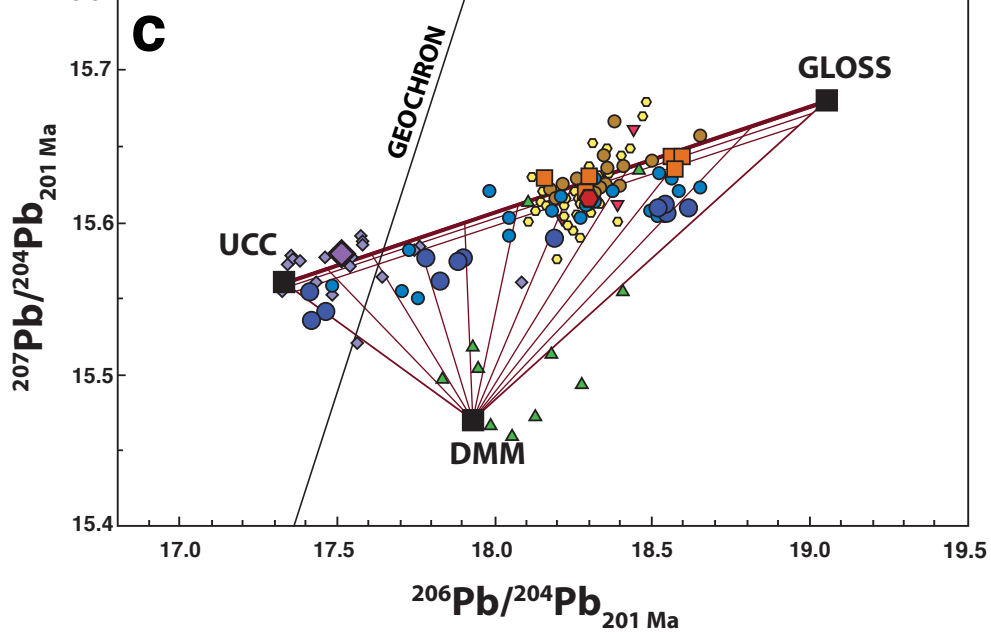
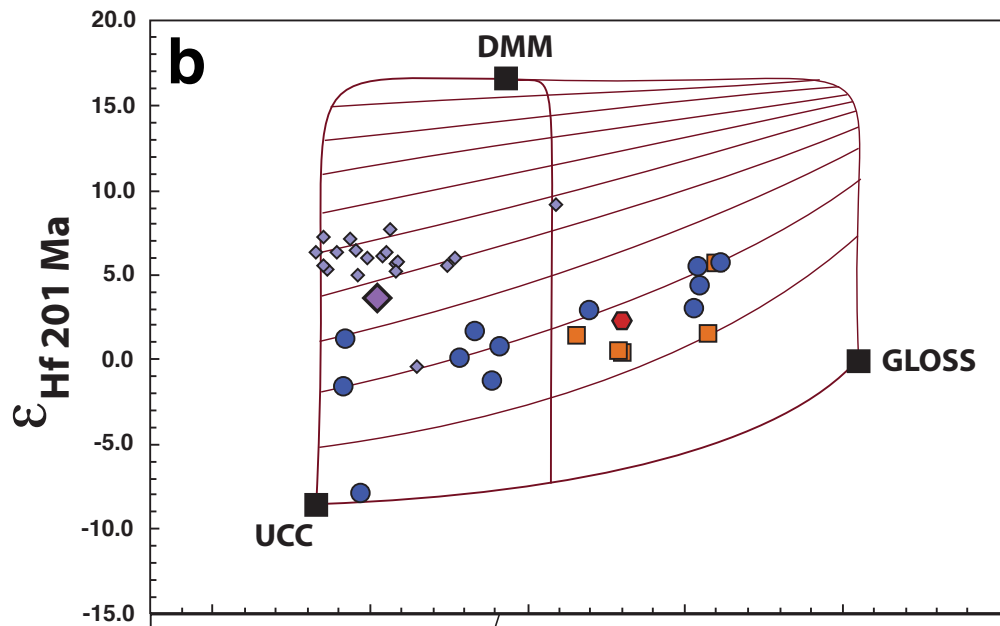
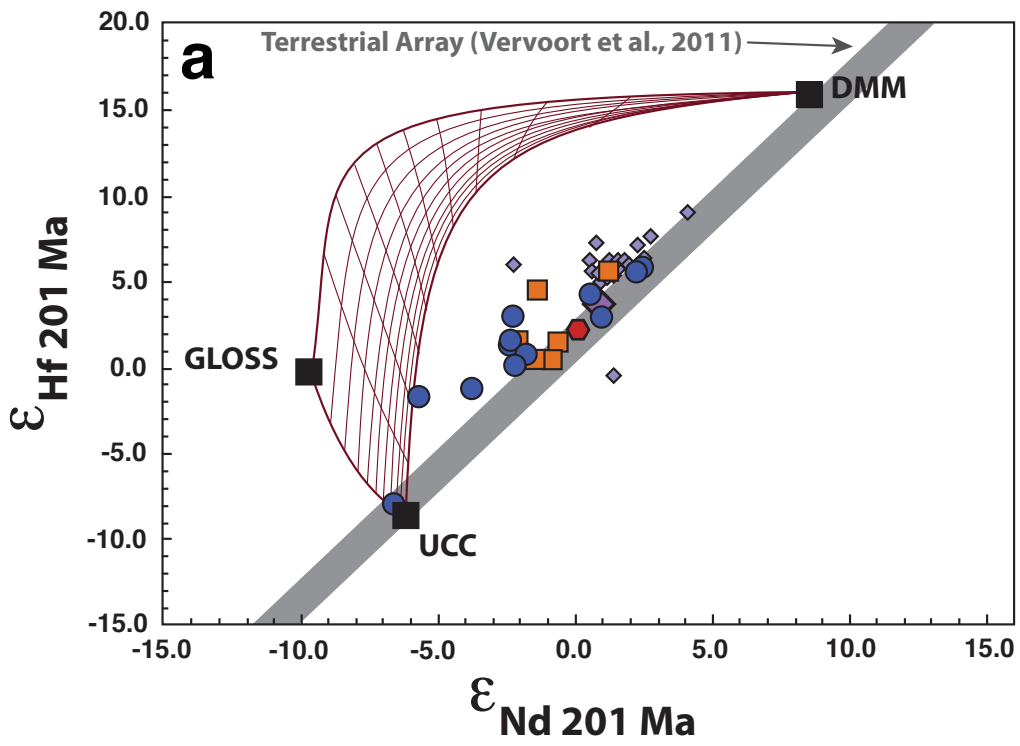


Figure 5.

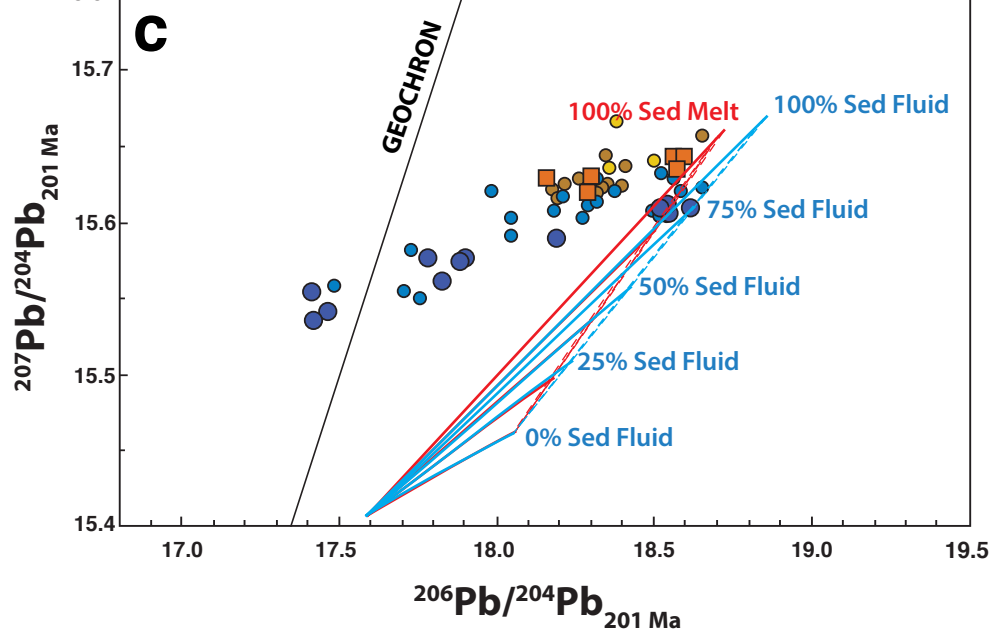
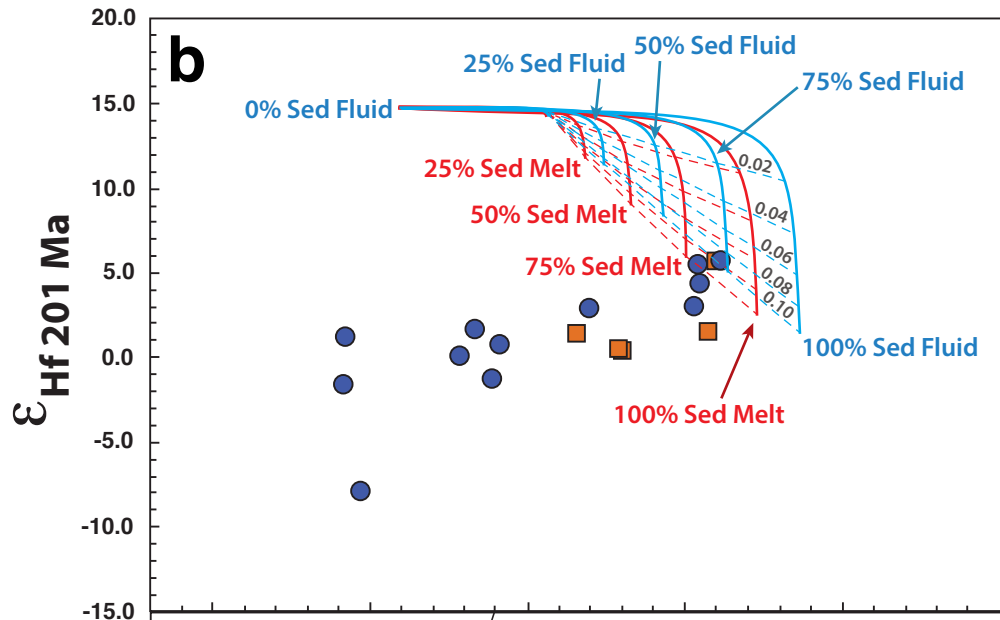
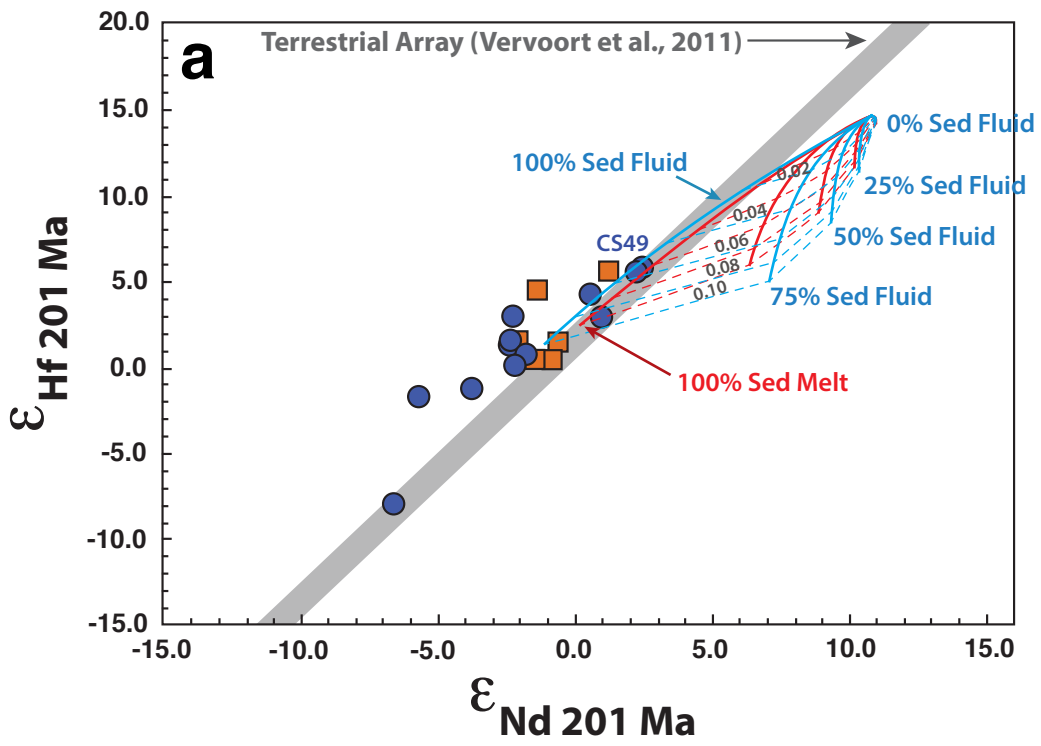


Figure 6.

